Article (discoveries)

Selective constraints on coding sequences of nervous system genes are a major determinant of duplicate gene retention in vertebrates

Julien Roux[1,2,*], Jialin Liu[1,2], Marc Robinson-Rechavi[1,2,*]

[1]Université de Lausanne, Département d'Ecologie et d'Evolution, Quartier Sorge, 1015 Lausanne, Switzerland

[2]Swiss Institute of Bioinformatics, Lausanne, Switzerland.

[*]Corresponding authors: julien.roux@unil.ch; marc.robinson-rechavi@unil.ch

Keywords

Whole-genome duplication, small-scale duplication, neuron, anatomy, gene expression, protein misfolding

Running title

Biased retention of vertebrate nervous system duplicates

Abstract

The evolutionary history of vertebrates is marked by three ancient whole-genome duplications: two successive rounds in the ancestor of vertebrates, and a third one specific to teleost fishes. Biased loss of most duplicates enriched the genome for specific genes, such as slow evolving genes, but this selective retention process is not well understood.

To understand what drives the long-term preservation of duplicate genes, we characterized duplicated genes in terms of their expression patterns. We used a new method of expression enrichment analysis, TopAnat, applied to *in situ* hybridization data from thousands of genes from zebrafish and mouse. We showed that the presence of expression in the nervous system is a good predictor of a higher rate of retention of duplicate genes after whole-genome duplication.

Further analyses suggest that purifying selection against protein misfolding, which is particularly strong in non-renewing neural tissues, likely constrains the evolution of coding sequences of nervous system genes, leading indirectly to the preservation of duplicate genes after whole-genome duplication. Whole-genome duplications thus greatly contributed to the expansion of the toolkit of genes available for the evolution of profound novelties of the nervous system at the base of the vertebrate radiation.

Introduction

The process of gene duplication plays a major role in the evolution of genomes, as it provides raw material for innovation (Lynch, Conery 2000; Conant, Wolfe 2008; Van de Peer, Maere, Meyer 2009). But only a minority of the gene duplication events reach fixation in a species, and survive in the long term with two functional gene copies (Innan, Kondrashov 2010). It is not yet clear what factors drive this process of selective retention, but it is clear that it is non random (Davis, Petrov 2004).

Focusing on whole-genome duplication events allows quantification of the long-term retention bias alone, the whole gene set having been fixed in duplicate (Singh et al. 2012). In vertebrates, it has been estimated that only 10 to 20% of the duplicates (or "ohnologs") that originated from the ancient whole-genome duplications at the origin of the lineage ("2R" hypothesis)(Ohno 1970; Holland et al. 1994; Hughes 1999; Putnam et al. 2008) or in teleost fishes ("3R" hypothesis)(Jaillon et al. 2004; Meyer, Van de Peer 2005) were eventually retained in the long term (Brunet et al. 2006; Nakatani et al. 2007; Putnam et al. 2008; Smith, Keinath 2015). These genes were shown to constitute a very biased subset of the genome. For instance, their protein sequences tend to be under strong selective constraint (Davis, Petrov 2004; Brunet et al. 2006; Howe et al. 2013). They tend to be involved in functions such as signaling, cognition and behavior, or regulation of transcription (Brunet et al. 2006; Putnam et al. 2008; Kassahn et al. 2009; Huminiecki, Heldin 2010; Schartl et al. 2013), and are expressed late in development (Roux, Robinson-Rechavi 2008). The causal mechanisms linking such properties to increased retention after whole-genome duplication have not been fully clarified so far.

An interesting study found that in yeast and *Paramecium*, the expression level of genes was a major determinant of their duplication retention rate after whole-genome duplication (Gout et al. 2010), an effect that could not be explained indirectly by other factors. This observation is noteworthy since gene expression level is also known to be a major determinant of the rate of protein evolution across a wide range of species (Drummond et al. 2005; Gu, Su 2007; Drummond, Wilke 2008).

The generalization of this result to vertebrates is complicated by their complex anatomy. One way to address this complexity is to investigate whether patterns of expression over anatomy could be linked to ohnolog retention rates. But surprisingly this question has rarely been addressed. Based on EST data, a study found little association between expression breadth – the number of tissues in which a gene is expressed – and retention rate after the 2R

whole-genome duplication (Satake et al. 2012). However, the authors observed lower retention of the fast-evolving genes expressed in endodermal tissues, such as the digestive tract, compared to slow-evolving genes expressed in ectodermal tissues, such as the nervous system. The expression patterns were opposite for small-scale duplication events, in agreement with other results showing that these two types of duplications tend to affect opposite sets of genes (Davis, Petrov 2005; Makino, Hokamp, McLysaght 2009).

These observations suggest that anatomical expression patterns of genes might help to understand the process of ohnolog retention in vertebrates. Unfortunately the techniques used to study gene expression patterns on a genomic scale, previously ESTs and microarrays, and more recently RNA-seq, usually lack anatomical precision. In this paper we took advantage of bioinformatics integration of another source of expression data, *in-situ* hybridizations. Expression patterns obtained with this technique are very precise, sometimes down to the cellular resolution (Lein et al. 2007; Diez-Roux et al. 2011; Jacobs, Albertson, Wiles 2011). They are also very inclusive, since it is possible to visualize the expression of a particular gene in the entirety of anatomical structures present in a histological section or even an entire organism ("whole-mount" *in-situ* hybridizations), without selecting *a priori* a tissue to dissect. Compared to other techniques, there is also less averaging or dilution of the expression signal for genes whose expression is heterogeneous among the cells or substructures of a tissue (Altschuler, Wu 2010; Pantalacci, Semon 2015).

A drawback of *in-situ* hybridizations, however, is that they usually give information on only one, or sometimes a handful of genes. Fortunately, there have been several efforts to generate with this technique high-throughput atlases of gene expression patterns in model organisms, notably zebrafish and mouse (e.g., Neidhardt et al. 2000; Thisse et al. 2004; Lein et al. 2007; Diez-Roux et al. 2011). Thus, there are thousands of *in-situ* hybridizations publicly available, allowing us to perform analyses at the genomic scale. Even more valuable, the expression patterns revealed by these hybridizations have been manually annotated to terms from anatomical ontologies, notably the cross-species ontology Uberon describing anatomical structures and their relationships in animals (Hayamizu et al. 2005; Sprague et al. 2006; Bastian et al. 2008; Mungall et al. 2012; Hayamizu et al. 2013; Haendel et al. 2014).

To detect the biases in anatomical expression patterns of ohnologs, we developed a novel bioinformatics approach. Similarly to the widely used functional enrichment tests performed on categories of the Gene Ontology (Ashburner et al. 2000; Yon Rhee et al. 2008), we used a Fisher's exact test to detect an enrichment in the proportion of ohnologs expressed in each anatomical structure of the organism. This methodology allowed us to monitor

expression biases with great precision, and to benefit from the information encoded in the ontology (e.g., parent-child relationships).

We observed that genes expressed in the nervous system had an increased chance of being retained after whole-genome duplication, whereas they had a decreased chance of being duplicated via small-scale duplication. This novel and robust observation helped us clarify the gene properties that causally influence the retention of duplicate genes. The rate of non-synonymous substitutions of nervous-system genes, their level of optimization of synonymous codon usage at site that are important for the protein structure stability, and their maximum level of expression across neural tissues are significantly associated to retention rate, suggesting a major role of selection against protein misfolding on ohnolog retention in vertebrates. We propose that purifying selection on coding sequences of nervous system genes, primarily preventing them from producing toxic misfolded protein products, could have the unexpected consequence of lowering their probability of loss of function, leading to their evolutionary long-term retention.

This model is consistent with a model proposed to explain the counterintuitive expansion of human disease-causing genes after the 2R whole-genome duplication events (Singh et al. 2012; Malaguti, Singh, Isambert 2014), and is not exclusive of previously proposed models, e.g., sub- or neo-functionalization (Ohno 1970; Force et al. 1999; He, Zhang 2005), the dosage-balance hypothesis (Freeling, Thomas 2006; Makino, McLysaght 2010; Birchler, Veitia 2012; Singh et al. 2012), or selection for absolute dosage (Osborn et al. 2003; Innan, Kondrashov 2010). Rather it expands these models to illustrate the key role of anatomy in shaping the duplicated gene content of vertebrate genomes.

Results

3R ohnologs are biased for nervous system expression

Zebrafish 3R ohnologs were identified using a phylogenomics approach, and were used as input gene list in an expression enrichment test (Materials and Methods, Figure S1). The list of anatomical structures showing enrichment for expression of these genes is shown in Table 1. At a false discovery rate (FDR) threshold of 10%, 25 structures were significantly enriched. The only significant depletion was for “unspecified”, a term indicating that the gene expression was assayed, but no anatomical structure was specified by the author.

A high fraction of the enriched anatomical structures were neural (e.g., sub-parts of the telencephalon, cerebellum, epithalamus, neuromast, retinal neural layer). To test whether

this did not simply reflect the structure of the Uberon anatomical ontology, which could use more terms to describe the nervous system than other anatomical systems, we made the inventory of all nervous system structures described in the ontology. We built two lists, a broad one also including sensory systems as well as embryonic precursors of nervous structures, and a more strictly defined list ("broad" and "strict" lists; see Materials and Methods). Out of the 25 structures showing an enrichment of expression of 3R ohnologs, 19 were part of the broad list of nervous system structures, of which 15 were part of the strict list. These proportions were significantly higher than the proportion of nervous system structures among all tested structures (Fisher's exact tests; broad list: p=0.0001, with odds-ratio=5.41; strict list: p=3.2e-5, odds-ratio=5.67). Even among structures that were not part of the nervous system, some still shared the same ectoderm developmental origin as nervous system (e.g., "ear vesicle" or "integument").

We applied the same procedure to other anatomical systems (see Materials and Methods), but all of them were under-represented. We also verified that the over-representation of nervous system structures was not dependent on the FDR threshold used in the enrichment analysis. In the rest of the article we describe the ontology enrichment results obtained at a FDR threshold of 10%, and we use the broad list of nervous system structures as reference.

We next turned to singleton genes (genes whose duplicate copy was lost after the 3R whole-genome duplication), and investigated if these were preferentially expressed in any anatomical structure. We found only two structures enriched for this group of genes: "unspecified" and "alar plate midbrain". However, 35 structures were significantly depleted in expression of singletons (Table S2), of which 22 were part of the nervous system (Fisher's exact test; p=0.0024, odds=2.89)

In summary, we observed that genes retained in duplicate after the fish-specific ("3R") whole-genome duplication were strongly biased for nervous system expression (in very diverse structures, including developmental precursors and sensory organs), whereas genes that were not retained in duplicate had the opposite tendency to not show expression in these structures. We reproduced these analyses using an independent dataset of 3,212 and 10,415 zebrafish 3R ohnologs and singletons identified using phylogenetic and synteny analyses (Braasch et al. 2016), and obtained consistent results (Tables S3 and S4).

Pre- or post-duplication bias?

These results could be explained by a duplicate retention bias, i.e., genes expressed in the nervous system before 3R were more likely retained as ohnologs. Or they could be explained by a bias in post-duplication evolution, i.e., ohnologs were more likely to acquire expression in the nervous system. To disentangle these two scenarios, it is possible to focus on an outgroup species that did not experience the whole-genome duplication, and compare the properties of orthologs of ohnologs and orthologs of singletons in this species, as a proxy for the pre-duplication properties of zebrafish genes (Davis, Petrov 2004; Brunet et al. 2006; Roux, Robinson-Rechavi 2008). The mouse represents a convenient such outgroup, since a large number of *in-situ* hybridization data are also available for this species, allowing to test the enrichment of expression in anatomical structures using the same methodology (see Materials and Methods).

We found that mouse orthologs of zebrafish 3R ohnologs were enriched for expression in 57 anatomical structures, among which 46 were nervous system structures (Table S5; p=1.6e-19, odds=13.9). In parallel, mouse orthologs of 3R singletons were significantly depleted for expression in two nervous structures, “olfactory cortex mantle layer” and “CA2 field of hippocampus”, and just above significance threshold, nervous system structures were also almost exclusively present at the top of the list (Table S6).

These results, consistent with the observations in zebrafish, suggest that the nervous system enrichment can be explained by an ohnolog retention bias, and that expression patterns before the 3R whole-genome duplication, or in an outgroup, can predict this retention bias.

The nervous system bias is weakly detected for 2R ohnologs

We repeated the enrichment analysis with mouse 2R ohnologs identified by phylogenomics, but these genes did not show any significant enrichment (Table S7). However, there was a significant enrichment for nervous system structures when we used an independent list of 5,376 mouse 2R ohnologs (Singh, Arora, Isambert 2015), identified using synteny comparison across multiple genomes (Table S8; 91 nervous structures out of 297 enriched structures; p=0.0081, odds=1.44).

Mouse 2R singletons were depleted in 107 structures, 31 of which belonged to the nervous system (Table S9). This slight over-representation of nervous system structures was however not significant (p=0.25, odds=1.29).

In summary, the results from the 2R whole-genome duplications were consistent with the 3R whole-genome duplication. Several technical factors could account for the fact that the 2R trends were weaker than the 3R trends, notably the older age of these events, but also post-duplication evolution patterns confounding this analysis that was not performed in an outgroup species.

Small-scale duplications

We also investigated whether an anatomical expression bias existed for duplicate genes that arose from other sources than whole-genome duplications, i.e., small-scale duplications. Because there was no whole-genome duplication in the phylogenetic branches leading to the zebrafish and mouse lineages, after 3R and 2R respectively, we isolated duplicates dated to these branches as small-scale duplicates. We removed those that were specific to these species since they could still be polymorphic or represent errors in the genome assemblies (Materials and Methods). Unfortunately, the small number of genes identified (385 and 646 duplicate genes for zebrafish and mouse respectively) probably led to low power of the enrichment test. In both species, we did not detect any significantly enriched or depleted anatomical structure. In mouse, the depletion results were close to significance, and we noticed numerous nervous system structures present at the top of the list (Table S10). Using an external curated list of small-scale duplicate pairs specific to rodents (Farre, Alba 2010), there were four structures with a significant expression enrichment ("placenta", "stomach glandular region mucosa", "ectoplacental cone" and "cardia of stomach") and 8 structures with a significant depletion, 7 of which were part of the nervous system (p=0.0003, odds=22.1; Table S11). Overall, there was weak evidence for a nervous system expression bias of small-scale duplicates.

Validation with microarray data

To check whether the expression biases could be observed with other types of expression data, we retrieved a microarray dataset in mouse that included samples from multiple nervous and non-nervous tissues (see Materials and Methods). We called the genes expressed or not in each sample, and ranked the tissues based on the proportion of mouse orthologs of zebrafish 3R ohnologs expressed (Figure 1A). We observed that the samples expressing the highest proportion of orthologs of ohnologs belonged to the nervous system. This result was confirmed with another microarray dataset (Figure S2A), and with human RNA-seq data from the GTEx consortium (Figure S2B).

Across neural tissues, there was little variation in the proportion of orthologs of ohnologs expressed, confirming that this bias was general to the whole nervous system. Only a few neural tissues stood out with lower proportions, notably the pituitary gland (Figure 1A, S2A and S2B). An independent microarray dataset, including samples from 46 neural tissues confirmed that the pituitary gland, but also the pineal body, displayed a lower proportion of orthologs of ohnologs expressed (Figure S2C). Interestingly, these tissues also stood out from clustering analyses based on expression levels across numerous nervous tissues (Zapala et al. 2005; Kasukawa et al. 2011), possibly because of their secretory activities (Gu, Su 2007) or different cell type composition.

Finally we ranked tissues based on the proportion of small-scale duplicates expressed, and observed an opposite picture: tissues expressing the lowest proportion of small-scale duplicates belonged to the nervous system (Figure 1B), supporting the weak trend observed with *in situ* hybridization data.

The rate of protein sequence evolution is associated with ohnolog retention

The nervous system expression bias could be an indirect effect of others factors driving differential retention of duplicate genes. For example, it was observed that genes with slow rates of amino acid substitution were more retained as ohnologs (Davis, Petrov 2004; Brunet et al. 2006). Since genes expressed in the nervous system also tend to be slowly evolving (Duret, Mouchiroud 2000; Gu, Su 2007; Drummond, Wilke 2008; Kryuchkova-Mostacci, Robinson-Rechavi 2015), the rate of amino acid substitutions could be a confounding factor behind the expression bias.

We first verified using our dataset that slowly evolving mouse genes. The 10% genes with the lowest non-synonymous substitutions rate values (d_N, calculated from pairwise comparisons of mouse-rat orthologs) were indeed significantly enriched for expression in nervous structures (Table S12; p=8.9e-7, odds=2.13). We also verified that mouse orthologs of zebrafish 3R ohnologs had a lower d_N than orthologs of singletons (Figure 2A). We then sub-divided the orthologs based on their expression in the nervous system, and surprisingly, while the pattern of slower rate of evolution of orthologs of ohnologs held among nervous system genes, it did not among non-nervous system genes (Figure 2B), and this could not be accounted by power issues (Supplementary text).

This result indicates that the relation between retention rates and sequence evolution rates is mainly caused by nervous system genes. This was confirmed when we split nervous system and non-nervous system genes into 10 equal-sized bins of d_N (i.e., bins with equal

numbers of genes): the proportion of orthologs of ohnologs in each bin was significantly associated with d_N for nervous system genes, but not so for non-nervous system genes (Figure 3A).

Highly expressed nervous system genes are more retained as ohnologs

The major hypothesis to explain the slow rates of sequence evolution of nervous-system genes is that their protein sequence was optimized for high translational robustness over the course of evolution (Drummond et al. 2005; Drummond, Wilke 2008; Zhang, Yang 2015). The choice of amino acid has been shown to facilitate protein folding (Yang, Zhuang, Zhang 2010; Wang 2016). Amino acid substitutions can thus destabilize protein structures, leading to increased levels of misfolded proteins. These can be toxic to cells because they are prone to aggregate to other proteins and to hydrophobic surfaces such as membranes (Drummond, Wilke 2008). The long lifetimes and high membrane surface area of neurons makes them particularly vulnerable to damages of misfolded proteins, explaining why the amino-acid sequences of nervous system genes are optimized and highly conserved (Drummond, Wilke 2008; Drummond, Wilke 2009; Biswas et al. 2016). We verified using our dataset that the negative correlation between d_N and expression levels was indeed markedly stronger in nervous tissues compared to other tissues (Figure S3A)(Duret, Mouchiroud 2000; Drummond, Wilke 2008; Kryuchkova-Mostacci, Robinson-Rechavi 2015).

We then tested whether the association between d_N and retention rates could be driven by the expression level of genes in the nervous system. To summarize the expression of genes across nervous system tissues, we considered their mean or maximum expression level across the 102 samples from 46 nervous tissues from the GSE16496 microarray experiment (Figures S3B, S4A and S4B). We then split genes into ten equal-sized bins of mean and maximum nervous system expression level. The proportion of mouse orthologs of zebrafish 3R ohnologs in the bins was significantly associated with maximum, but not with mean nervous system expression (Figure S5A). Interestingly, the association with maximum nervous expression was maintained when we controlled for d_N by repeating the same analysis on genes with the highest or lowest d_N (Figure S5B; although the trend for low d_N genes was slightly below the significance threshold). Conversely the association between d_N and retention rate disappeared when we controlled for maximum nervous expression by repeating the d_N analysis on genes with the highest or lowest maximum nervous expression level (Figure S5C). A small residual d_N trend was visible: if maximum nervous expression perfectly controlled for d_N, the two regression lines would be overlapping on Figure S5B, and they would be flat on Figure S5C.

In summary, for nervous system genes, the maximum level of expression in nervous tissues is clearly associated with higher rates of ohnolog retention. It is difficult though from these results alone to assess whether this association is direct or indirectly caused by the association of both factors to d_N.

Selective constraints at synonymous sites also influence ohnolog retention

The association of retention rates with d_N, and with maximum nervous expression, suggests a potential link with selection against protein misfolding. Another manifestation of this selective force is the optimization of translational robustness through selection on synonymous codon usage (Drummond, Wilke 2008). Codons binding their cognate tRNA with higher affinity than non-cognate competitors are translated more accurately, decreasing the chances of incorporation of wrong amino acids that could destabilize protein structures. The selection to maintain a state of optimized synonymous codon usage is apparent in the association between d_N and d_S (Figure S4C), and in the stronger negative correlation between the rate of synonymous substitutions (d_S) and expression levels in nervous tissues compared to other tissues (Figure S6A). However we did not observe any relation between the proportion of mouse orthologs of zebrafish 3R ohnologs and d_S (Figure S6B).

This may be explained by the fact that selection against protein misfolding does not act on synonymous codon usage at all amino acid positions, but predominantly at those that are the most important for the structure of the protein (Drummond, Wilke 2008; Zhou, Weems, Wilke 2009). The strength of this effect can be quantified using Akashi's test, assessing how strong is the association between preferred codons and conserved amino acids, taken as a proxy of structurally important sites (Akashi 1994).

The odds ratio reflecting this association ("*Psi*" score) was only weakly correlated with both the rate of non-synonymous substitutions, d_N, and with maximum nervous expression (Figure S4E and F), but was more strongly associated with translation rates, calculated from ribosome profiling data in embryonic stem cells, embryonic fibroblasts or neutrophils (Dana, Tuller 2014)(see Materials and Methods; Figure S7). Genes showing the 10% highest *Psi* score were enriched for expression in the nervous system (p=0.00081, odds=1.98), and interestingly the top structures were almost exclusively developing ectodermal or neural structures (e.g., "rhombomere", "presumptive midbrain", "limb bud"; Table S13). In summary, the *Psi* score is capturing some aspect of selection against protein misfolding that seems largely independent of the constraints on amino acid sequences.

Interestingly, when we separated mouse genes in 10 equal-size bins of *Psi*, we observed a significant relation with the proportion of orthologs of ohnologs (Figure 3B). And similarly to the d_N trend, the association was supported for nervous system genes, but not for non-nervous system genes. Focusing on the nervous system genes, we checked whether the d_N and *Psi* trends were dependent (Figures 3C and D). The proportion of orthologs of ohnologs was the highest for the genes with the lowest d_N and the highest *Psi*, suggesting a positive interaction effect. Nervous system genes that had either high d_N or low *Psi* included around 10% of orthologs of ohnologs, similarly to non-nervous system genes, but nervous system genes that had both low d_N and high *Psi* included more than 30%.

In summary, genes with the strongest sequence constraints against protein misfolding, both at non-synonymous and at synonymous sites, were more retained in duplicate after whole-genome duplication.

The nervous system bias is independent from the dosage-balance hypothesis

The dosage-balance hypothesis was previously proposed to explain ohnolog retention after whole-genome duplication (Freeling, Thomas 2006; Makino, McLysaght 2010; Birchler, Veitia 2012; Singh et al. 2012). Groups of interacting genes, sensitive to relative dosage changes, (e.g., members of a protein complex, or genes belonging to the same metabolic pathway), could be maintained in duplicates because the loss of any gene of the group would lead to dosage imbalance and be detrimental. Notably, dosage imbalance is expected to impact the formation of protein complexes involving at least two different genes, and composed of at least three subunits (Veitia, Bottani, Birchler 2008), so genes involved in such complexes should be more retained after whole-genome duplication.

We tested this using protein complex data from the UniProtKB/Swiss-Prot database (The UniProt Consortium 2015), where complex type and number of subunits are precisely annotated. We split genes into six groups: genes involved in (i) monomers, (ii) homo-multimers and (iii) hetero-dimers, which should not be sensitive to dosage imbalance; (iv) genes involved in hetero-multimers with at least 3 subunits, which should be sensitive to dosage imbalance; (v) genes involved in uncharacterized complexes, which likely include some genes sensitive to dosage imbalance; and finally (vi) non-annotated genes. Genes annotated to several groups were kept in the group expected to be most sensitive to dosage imbalance (see Materials and Methods). We observed that the proportion of mouse orthologs of zebrafish 3R ohnologs was the highest for members of hetero-multimer complexes, consistent with the dosage-balance hypothesis (Figure S8A). This effect was independent

from nervous system expression, since it was observed both for nervous and non-nervous system genes. When controlling for d_N, we observed a positive interaction between the two effects: members of hetero-multimer complexes that had low d_N were the most retained (Figure S8B).

Another manifestation of the dosage-balance hypothesis could be selection to maintain stoichiometry within metabolic pathways. Previous studies in *Paramecium* and *Arabidopsis* have reported that the retention of genes involved in metabolic pathways differed across timescales, and was higher than other genes for recent whole-genome duplication events, while it was lower for ancient events (Aury et al. 2006; Gout, Duret, Kahn 2009; Bekaert et al. 2011). Consistent with these observations, we observed a lower proportion of mouse orthologs of zebrafish 3R ohnologs among genes involved in metabolic processes (Figure S9), both for nervous and non-nervous system genes, confirming that there is no long-term action of selection against dosage imbalance on whole pathways.

Finally, we examined the relation between the level of protein connectivity and retention rates. The number of protein-protein interactions was previously taken as a proxy for sensitivity to dosage imbalance (Prachumwat, Li 2006; Flagel, Wendel 2009; Rodgers-Melnick, Culp, DiFazio 2013; Cuypers, Hogeweg 2014). We observed that mouse orthologs of zebrafish 3R ohnologs had a significantly higher connectivity than orthologs of singletons (Figure S10A), in agreement with previous studies (Hakes et al. 2007; Liang, Li 2007; Rodgers-Melnick et al. 2012). But similarly to the d_N trend, when we sub-divided genes based on their expression pattern, the trend held only for nervous system genes. Since highly connected genes tend to display a lower d_N (Figure S4G), we tested whether this trend could be explained by d_N differences: this was not the case, with both trends even positively interacting (Figure S10B and C). Similarly, the connectivity trend could not be explained by other weakly correlated factors, maximum nervous expression and *Psi* score (Figure S4I and H), but it disappeared when we split genes based on their annotation to different complex subtypes (Figure S10D).

This suggests that the connectivity trend could indeed be explained by higher dosage sensitivity of most highly connected genes, although there is no clear *a priori* reason for the trend to be seen only among nervous system genes (see Discussion).

Small-scale duplication is not associated to the same underlying factors

Small-scale duplicates have often been observed to behave in an opposite way to ohnologs, a pattern that we confirmed with the lower rate of duplication of genes expressed in

the nervous system (Fig. 1B). More careful examination indicated that this bias was not caused by the same underlying factors as ohnologs.

First, there was a difference in d_N values between genes that experienced a small-scale duplication event and other genes, but this was true both for nervous system and non-nervous system genes (Figure S11A). This suggests that the depletion for nervous system expression might just be an indirect consequence of the association between small-scale duplication and sequence evolution rates. Second, the relation between the proportion of small-scale duplicates and d_N was best explained by a linear fit, whereas the best model was a log-linear trend for ohnologs (Figure S11B). Third, there was no relation between the proportion of small-scale duplicates and *Psi* score, suggesting that selection against protein misfolding had no effect on small-scale duplication patterns (Figure S11B and C).

Since expression level is a major determinant of d_N, we examined the relation between the proportion of small-scale duplicates and summaries of expression levels across nervous and non-nervous tissues. The best trend was obtained using the mean expression across all available tissues (not only nervous tissues; Figure S12A), and this effect was in positive interaction with d_N: the most highly duplicated genes displayed both a low mean expression and a high d_N (Figure S12B and C).

We finally tested the dosage-balance hypothesis on small-scale duplicates, using protein complex information. In comparison to whole-genome duplication patterns (Figure S8), hetero-multimer genes displayed a lower proportion of duplicates, consistent with their dosage-sensitivity (Figure S13), but this was only true for nervous system genes. For the subset of non-nervous system genes, the proportion of duplicate hetero-multimer genes was surprisingly higher than the other groups of genes. Given that this category includes the lowest number of genes, this pattern must be interpreted carefully. The low number of small-scale duplicates makes it unfortunately difficult to reliably test the dependency of this trend with respect to the d_N and mean expression level trends.

Discussion

In this study we took advantage of thousands of high quality *in situ* hybridization data describing precisely mouse and zebrafish gene expression patterns. These are mapped to ontologies describing the anatomy of these species, making it possible to perform ontology enrichment tests and to detect tissues enriched for the expression of genes of interest. This methodology corrects for biases in annotation and in data availability, i.e., some anatomical structures are better annotated than others (Yon Rhee et al. 2008).

We uncover a strong and robust trend whereby genes expressed in neural tissues are more likely retained in duplicate after whole-genome duplication. These same genes are less likely to duplicate via small-scale duplication events. To our knowledge, this result was never previously reported, but is fully consistent with previous studies. For example, ohnologs were found enriched for Gene Ontology terms related to signaling, behavior, neural activity or neurodevelopment (Brunet et al. 2006; Putnam et al. 2008; Roux, Robinson-Rechavi 2008; Kassahn et al. 2009; Huminiecki, Heldin 2010; Howe et al. 2013; Schartl et al. 2013), which are typical nervous system genes functions. The slow rate of sequence evolution of ohnologs (Davis, Petrov 2004) can also be explained by the tendency of nervous system genes to evolve slowly (Duret, Mouchiroud 2000; Gu, Su 2007; Drummond, Wilke 2008).

Surprisingly, there have been few previous analyses of ohnolog retention biases with respect to gene expression patterns, probably because of the limited anatomical resolution of most microarray and RNA-seq datasets, and the difficulty in gathering many *in situ* hybridization experiments for an integrated analysis. Satake and colleagues (2012) reported that the proportion of 2R ohnologs detected in EST datasets was the highest in ectoderm-derived tissues, while the proportion of small-scale duplicates was the lowest, which is consistent with our observations.

Once this pattern was established, the next challenging task was to disentangle, within the network of factors associated with retention rates, which factors could be causal, and more broadly, which mechanisms are in action (Drummond, Raval, Wilke 2006; Singh et al. 2012; Kryuchkova-Mostacci, Robinson-Rechavi 2015). The rate of non-synonymous substitutions, d_N, is closely associated to the maximum level of expression across nervous tissues, an association that is likely caused by selection against protein misfolding (Drummond, Wilke 2008). Interestingly, both factors are associated with retention of nervous system ohnologs, suggesting that selection against protein misfolding could play a key role in this process. This hypothesis is corroborated by the observation that another manifestation of selection against protein misfolding, the optimization of codon usage at structurally sensitive sites, is also associated with retention rates, and this effect is not controlled by d_N or maximum nervous system expression. These effects even seem to be in positive interaction: genes that have a low d_N, a high maximum nervous system expression and a high *Psi* score have the highest chances of retention.

After whole-genome duplication, duplicate gene loss starts with the fixation of loss-of-function mutations in one of the gene copies. This can occur neutrally as long as the gene function is backed-up by the other copy. Thereafter the non-functional copy accumulates

other substitutions and degenerates (Albalat, Canestro 2016). Such a neutral scenario might not be possible for nervous system genes whose sequence is constrained by selection against protein misfolding. Indeed, mutations occurring both at non-synonymous sites, and at some synonymous sites, can increase the rate of production of toxic misfolded proteins, and this deleterious effect should hamper their fixation in the population (Figure 4). This simple model can explain how both duplicate gene copies can be "protected" from degeneration by purifying selection after whole-genome duplication, despite functional redundancy.

More broadly than nervous system genes, any gene subject to dominant deleterious effects mutations should be more likely retained as ohnolog, since the organism would pass by a low fitness intermediate when losing one copy. In fact, Gibson and Spring (1998), and later Singh and colleagues (2012) proposed such a model to explain the puzzling observation that disease-causing genes were preferentially retained after the 2R whole-genome duplications (Gibson, Spring 1998; Makino, McLysaght 2010; Dickerson, Robertson 2012; Singh et al. 2012; Chen et al. 2013; Malaguti, Singh, Isambert 2014; Singh et al. 2014; Tinti et al. 2014). They later supported this model by theoretical population genetics work (Malaguti, Singh, Isambert 2014), explaining the accumulation of repertoires of "dangerous" genes after whole-genome duplication.

Of course, our model does not totally exclude the possibility of pseudogenization of nervous system genes. For example, a mutation introducing a stop codon at the very beginning of the coding sequence would circumvent the action of selection against protein misfolding. It is also possible that regulatory mutations silence one copy, opening the way to its neutral degeneration (Thompson, Zakon, Kirkpatrick 2016). The neutral evolution of asymmetric expression levels between duplicate copies has indeed been reported (Gout, Lynch 2015; Lan, Pritchard 2016). But (i) this process was shown to require substantial amounts of time, and (ii) the evolution of expression levels in the nervous system is tightly controlled and slower than in other tissues (Pennacchio et al. 2006; Brawand et al. 2011; Barbosa-Morais et al. 2012; Merkin et al. 2012). Hence, there is little reason to think that other pseudogenization routes would compensate the deficit of losses for nervous system ohnologs.

Our model also does not exclude the possibility that some ohnolog pairs are retained through the action of previously described mechanisms (Innan, Kondrashov 2010), for example sub-functionalization (Force et al. 1999) or neo-functionalization (Ohno 1970; He, Zhang 2005). However we could not find any reasonable explanation for the nervous system retention bias using these alternative mechanisms. They might however be necessary on

different time scales, to maintain ohnologs in the long term. For example, nervous system duplicates that avoided rapid initial loss could be eventually retained because they evolved new functions later in time (Kassahn et al. 2009; Chen et al. 2011).

Another interesting model is the dosage-balance hypothesis, which was proposed to be a major determinant of duplicate gene retention after whole-genome duplication, at least on short evolutionary time scales (Papp, Pal, Hurst 2003; Freeling, Thomas 2006; Makino, McLysaght 2010; McLysaght et al. 2014; Thompson, Zakon, Kirkpatrick 2016). This hypothesis is difficult to test in vertebrates because there are only a few, noisy, datasets allowing to assess the sensitivity of genes to dosage imbalance. Previous studies have sometimes relied on indirect evidence, for example, it was found that genes with high levels of protein-protein interactions (more connected genes) tended to be more retained after whole-genome duplication, which was interpreted as an evidence that these genes are more sensitive to changes in dosage (Liang, Li 2007; Rodgers-Melnick, Culp, DiFazio 2013).

Such an interpretation is subject to caution. Although we indeed found connectivity to be significantly associated with retention rates, we noticed that the trend was only supported for nervous system genes. There is no reason to expect this pattern from the dosage-balance hypothesis. Interestingly, it was previously shown that in addition to the optimization of amino acid sequences against protein misfolding, sequences were also optimized to reduce the levels of misinteractions with other proteins (Yang et al. 2012). Protein surface residues in particular are optimized for decreased stickiness and misinteractions, which are deleterious because they waste functional molecules, can interfere with functional interactions, or initiate damaging cellular processes (Zhang, Maslov, Shakhnovich 2008; Vavouri et al. 2009; Yang et al. 2012). The chances of detrimental effect might be higher for highly connected proteins, and similarly to protein misfolding, the effects might be more detrimental to non-renewing neural cells than other cell types, contributing to a retention bias of highly connected nervous system ohnologs. Hence, this mechanism provides an alternative explanation, probably complementary to the dosage-balance hypothesis, to the relation between connectivity and retention rates.

A better source of evidence to test the dosage-balance hypothesis is protein complex data. But different complex subtypes are not equally sensitive to dosage imbalance (Veitia, Bottani, Birchler 2008). When separating complexes into permanent or transient complexes, a previous study in human surprisingly observed that the retention rates after the 2R whole-genome duplications were lower for permanent complexes, despite their higher susceptibility to dosage-balance constraints (Singh et al. 2012). We separated genes into those involved or

not in dosage-sensitive complexes and, consistent with the dosage-balance hypothesis, observed a higher retention of the former. Moreover, this trend was supported both for nervous system and non-nervous system genes, and was independent of confounding factors such as d_N. Another analysis performed with another source of data gave somewhat conflicting results, but the annotations were less comprehensive and precise (see Supplementary Text). Overall, more work is needed to bring clearer support to the dosage-balance hypothesis. Of note, it is important to be careful with data transferred across species, which could be biased by the rates of sequence evolution, and to study pre-duplication biases in an outgroup species, because duplication itself likely influences post-duplication evolution of dosage-sensitive genes (e.g., ohnologs might be more likely to evolve into hetero-multimer complexes members)(Musso, Zhang, Emili 2007; Qian, Zhang 2014).

Interestingly, it is worth noting that the dosage-balance hypothesis, quite similarly to our model of Figure 4, can explain duplicate retention biases by only invoking the action of purifying selection (Freeling, Thomas 2006), acting not on detrimental mutations in coding sequences as in our model, but on detrimental changes in expression of dosage-sensitive genes. The predominant role of purifying selection can account for the observation that ohnologs usually do not duplicate via small-scale duplication events. Indeed, small-scale duplication events first need to reach fixation in the population, a process that is rarely successful for such genes, whose mutations can be dominant negative (Innan, Kondrashov 2010; Singh et al. 2012).

We observed that small-scale duplicates were rarely expressed in the nervous system, but this was likely an indirect effect of low fixation and retention rates of duplicates of highly expressed genes, which evolve slowly. This is consistent with purifying selection acting primarily on the deleterious effects of doubling the gene expression induced by small-scale duplications (Schuster-Böckler, Conrad, Bateman 2010; McLysaght et al. 2014). Although average expression level is highly correlated with d_N, it did not account for the entirety of the relation between d_N and rate of small-scale duplication. The additional effect of d_N could be due to post-duplication biases, that we did not control for in this analysis. Small-scale duplicates were indeed shown to experience an accelerated evolutionary rate after duplication, possibly associated with a process of sub- or neo-functionalization (Jordan, Wolf, Koonin 2004; Fares et al. 2013; Pegueroles, Laurie, Alba 2013). Finally, selection against protein misfolding was not associated with small-scale duplication rates. This is perhaps not surprising, because the sequence of genes expressed in tissues sensitive to protein misfolding

was optimized by natural selection, and duplication is unlikely to affect this, especially since the fixation phase of duplicates is probably too short for point mutations to accumulate.

Conclusion

The implications of our results are manifold. First, they confirm that whole-genome duplication is a unique type of evolutionary event, which enriches the gene set of a lineage with genes under strong purifying selection, e.g., dosage-sensitive genes, disease-causing genes, or nervous system genes. Mutations affecting the sequences or the expression of these genes can have clear detrimental consequences, adding a long term burden to genomes. Counter-intuitively, the preferential retention of these genes is driven by the action of purifying selection alone, although this is usually viewed as a protective force. Our study focused on vertebrates, but such a situation is most likely true for other organisms which experienced whole-genome duplications, such as plants or unicellular eukaryotes, although the sets of retained genes might differ.

On the other hand, whole-genome duplications have often been claimed to be beneficial in the long term, since the addition of new genes to genomes provides new material for evolution to act on, and increases evolvability of the lineages (Van de Peer, Maere, Meyer 2009; Kondrashov 2012; Cuypers, Hogeweg 2014). A particularly interesting example is the ancestral 2R event, which added to the genomes of vertebrates a large number of regulatory genes, such as transcription factors, as an indirect effect of purifying selection for gene dosage balance. Freeling and Thomas coined this phenomenon a "spandrel" of purifying selection, and suggested that it contributed to the increased morphological complexity of vertebrates (Gould, Lewontin 1979; Freeling, Thomas 2006).

Our results highlight that another such by-product of purifying selection is the enrichment of the vertebrate genomes for nervous system genes, at a time which coincided with major evolutionary novelties of the nervous system. The expanded toolkit of nervous genes likely provided opportunities for regulatory network rewiring and new functions to evolve (Evlampiev, Isambert 2007; Oakley, Rivera 2008; Chakraborty, Jarvis 2015). For example, it was suggested that the 2R events gave vertebrates the tools to evolve new structures such as the neural crest, placodes and a midbrain–hindbrain boundary organizer (Holland 2009). Similarly, in fish it was suggested that the 3R whole-genome duplication contributed to expand the toolkit of cognition-related genes that gave teleosts a high level of behavioral complexity compared to other groups of cold-blooded vertebrates such as amphibians and reptiles (Schartl et al. 2013).

Materials and Methods

Data files and analysis scripts are available on our GitHub repository: http://github.com/julien-roux/Roux_Liu_and_Robinson-Rechavi_2016

Mouse and zebrafish *in-situ* hybridization data

Mouse (*Mus musculus*) RNA *in-situ* hybridization expression data were retrieved from the GXD database (Smith et al. 2007; Smith et al. 2014) on December 2014. Wild-type data, obtained under non pathological conditions, and with no treatment ("normal" gene expression) were integrated into Bgee (http://bgee.org/), a database allowing the comparison of transcriptome data between species (Bastian et al. 2008). The data used in this article all come from the release 13 of Bgee. In Bgee, expression data are mapped to the Uberon anatomical ontology (http://uberon.org). The mapping from the EMAP (Bard et al. 1998) and MA (Hayamizu et al. 2005) mouse anatomical ontologies (onto which GXD *in-situ* hybridization data are mapped) to Uberon was obtained from Uberon cross-references. Terms from the EMAPA and MA ontologies that were not present in the Uberon ontology, but to which *in-situ* hybridization data were mapped were also included in the analyses.

Similarly, zebrafish (*Danio rerio*) *in-situ* hybridization expression data were retrieved from the ZFIN database (Sprague et al. 2006) on December 2014 and integrated into Bgee release 13 after mapping to the Uberon anatomical ontology. Terms from the ZFA ontology that were not present in the Uberon ontology, but to which *in-situ* hybridization data were mapped were also included in the analyses.

Mouse microarray data

Mouse microarray data and their mapping to the Uberon anatomical ontology were retrieved from Bgee release 13. We targeted experiments including a large number of samples from many different tissues, and including multiple nervous and non-nervous system tissues. We retained the accessions GSE3594, GSE10246 and GSE16496.

GSE3594 is a dataset composed of 129 samples from 24 neural tissues and 10 body tissues from different strains of inbred mice (Zapala et al. 2005). This experiment was hybridized to the Affymetrix Murine Genome U74A Version 2 array. Raw data (CEL files) were not available from GEO, so the normalized intensities and present/absent calls provided by the MAS5 software (Liu et al. 2002) were used.

GSE10246 corresponds to the GNF Mouse GeneAtlas V3 (Su et al. 2004) and there were 91 samples from 45 tissues (including 12 neural tissues, as well as 7 sub-structures of the eye) included into Bgee. This dataset was hybridized to the Affymetrix Mouse Genome 430 2.0 Array chip and was reprocessed through the Bgee pipeline (see http://bgee.org/bgee/bgee?page=documentation). Briefly, this includes normalization of the signal of the probesets by the gcRMA algorithm, and a Wilcoxon test on the signal of the probesets against a subset of weakly expressed probesets to generate present/absent calls (Schuster et al. 2007).

GSE16496 included expression data 102 samples from 46 regions of the mouse central nervous system (Kasukawa et al. 2011). This dataset was hybridized to the Affymetrix Mouse Genome 430 2.0 Array chip and also reprocessed through the Bgee pipeline.

We summarized the expression of genes across nervous system tissues by considering for each gene the mean, median or maximum of $\log_2$ signal across all samples from the GSE16496 experiment. Results were similar when using nervous tissue samples of the GSE3594 (not shown). Because results were similar using the median or the mean expression across nervous tissues, we only show results using the median.

Human RNA-seq data

Human RNA-seq data from the GTEx consortium (Melé et al. 2015; The GTEx Consortium 2015) were retrieved from Bgee release 14 (GTEx processed and annotated data available on ftp.bgee.org; full release planned in Feburary 2017). All samples were manually annotated to the Uberon ontology and only healthy samples were retained, based on metadata annotation (e.g., medical history or cause of death). There were 4,860 retained GTEx libraries, mapped to 75 different Uberon terms. The libraries were reprocessed through the Bgee pipeline to generate present/absent calls for each gene. Briefly, RNA-seq reads from each library were pseudo-aligned with Kallisto (version 0.42.4)(Bray et al. 2016) to the annotated human transcripts from Ensembl (release 84). Transcript-level TPM estimates were then summed at the gene level. Reads were also pseudo-mapped to a set of 28,573 intergenic regions, located at least 500 bp away from any genic region, and whose size ranged from 2000 bp to 20,000 bp. The “background” expression signal observed at these regions was used to set a TPM threshold for each library to determine presence/absence calls. At the threshold the ratio of the proportions of intergenic regions called present to the proportion of coding genes called present was set to 5%.

Identification of duplicates and singletons

Gene families were obtained from the Ensembl database release 79 (Hubbard et al. 2009). We used the Perl API to query the Ensembl Compara Gene trees (Vilella et al. 2009) and scan for gene trees with specific topologies. Notably we stringently selected sets of genes with or without duplications on specific branches of the vertebrate phylogenetic tree. We randomly picked a subset of gene trees to verify that they indeed displayed the expected topologies. Below is a description of the selected topologies, which are illustrated on Figure S1. These are dependent on the set of species integrated into Ensembl release 79, accessible at http://mar2015.archive.ensembl.org/info/about/speciestree.html. All genes lists are available as supplementary material (file gene_lists.zip) and scripts are available on our GitHub repository.

Fish-specific (3R) whole-genome duplication (Figures S1A, B, C and D)

We first selected subtrees with a basal speciation node dated at the Neopterygii taxonomical level. These subtrees include a spotted gar (*Lepisosteus oculatus*) outgroup, which did not experience the 3R duplication (Braasch et al. 2016), and teleost fish species, which experienced it. We classified zebrafish genes as confident 3R duplicates if the child node of the root of the subtree was a high confidence (score above 50%) duplication node dated at the Clupeocephala taxonomic level, followed by two speciation nodes dated at the Clupeocephala taxonomic level, each delineating a subtree containing no further duplication or loss on the branches leading to zebrafish (i.e., one zebrafish gene per subtree). We classified zebrafish genes as confident 3R singletons if the child node of the root of the subtree was a speciation node dated at the Clupeocephala taxonomic level, with no further duplication or loss on the branches leading to zebrafish. In total we obtained 2422 ohnologs, and 8973 singletons.

Of note, our identification of ohnologs is based on phylogeny alone, and does not use any synteny information. Small-scale duplicates that emerged on the Clupeocephala branch will be wrongly incorporated in the list of 3R ohnologs. Given relatively low rate of retention of duplicates originating from small-scale duplication (Lynch, Conery 2000), we ignored this problem in our analyses.

We classified mouse or human genes as confident orthologs of zebrafish 3R ohnologs if there was a two-to-one orthology relationship to a single mouse/human gene at the Euteleostomi taxonomical level. We classified mouse or human genes as confident orthologs of zebrafish 3R singletons orthologs if there was a one-to-one orthology relationship to a

single mouse/human gene at the Euteleostomi taxonomical level. In total we obtained 974 mouse orthologs of 3R ohnologs, 6,373 mouse orthologs of 3R singletons, 976 human orthologs of 3R ohnologs, and 6,358 human orthologs of 3R singletons.

Vertebrate (2R) whole-genome duplications (Figures S1E and F)

It is still debated whether one or two whole-genome duplication events occurred at the basis of vertebrates (Smith, Keinath 2015). In gene trees, we thus allowed for the possibility of one or two duplications at the basis of vertebrates. If two rounds of whole-genome duplication really occurred, this means that we required ohnologs of at least one event to be retained.

We first selected subtrees with a basal speciation node dated at the Chordata taxonomical level – or at the Bilateria taxonomical level when there was no chordate node in the subtree. We classified mouse genes as confident 2R duplicates if the child node of the root of the subtree was a high confidence duplication node dated at the Vertebrata taxonomic level, followed by an optional second high confidence duplication node dated at the Vertebrata taxonomic level, followed by two speciation nodes dated at the Vertebrata taxonomic level, each delineating a subtree containing only one mouse gene and including genes from at least two different fish species. We used Euteleostomi instead of Vertebrata to date the 2R duplications if there was no lamprey gene in the subtree. We classified mouse genes as confident 2R singletons if the child node of the root of the subtree was a speciation node dated at the Vertebrata/Euteleostomi taxonomic level, and delineated a single subtree including one mouse gene and genes from at least two different fish species. We could not enforce strictly the constraint that no duplication occurred in the tetrapod lineage on the branches leading to mouse, because Ensembl mammalian trees include a high number of dubious duplication nodes (duplication confidence score = 0) that are generated when the gene tree topology is not consistent with the species tree. Given the high number of mammalian species in Ensembl, this problem occurred in virtually each of the trees we examined. In total, we obtained 1389 2R ohnologs and 2999 singletons.

Small-scale duplications (Figures S1G and H)

We observed that genome assembly and annotation errors resulted in a high number of likely artifactual species-specific paralogs in gene trees. Thus we chose to retain only small-scale duplicates that originated before the split with at least one species. For zebrafish the more recently diverged sister species present in Ensembl was the cave fish *Astyanax*

mexicanus, so we focused on small-scale duplicates that originated on the Otophysa branch (deeper branches could not be considered because of the 3R fish-specific genome duplication). We first selected subtrees with a basal speciation node dated at the Clupeocephala taxonomical level. We then retrieved homology relationships between all zebrafish paralogous genes in the subtree (if any), and retained only the high-confidence ones, which did not involve paralogs with 100% sequence identity (probable assembly artifacts) or <10% sequence identity (probable gene split), and were dated at the Otophysa taxonomical level. In total we obtained 385 duplicates.

For mouse we focused on mammal-specific small-scale duplications. We first selected subtrees with a basal speciation node dated at the Mammalia taxonomical level. We then retrieved homology relationships between all mouse paralogous genes in the subtree (if any), and retained only the high-confidence ones, which did not involve paralogs with 100% sequence identity or <10% sequence identity, and were dated at the Theria, Eutheria, Boreoeutheria, Euarchontoglires, Glires, Rodentia, Sciurognathi, or Murinae taxonomical levels. In total, we obtained 646 duplicates.

Ontology enrichment analyses

Enrichment and depletion of expression in anatomical structures were tested with a Fisher exact test using a modified version of the R Bioconductor package topGO (http://bioconductor.org/; Adrian Alexa, pers. comm.)(Gentleman et al. 2004; Alexa, Rahnenfuhrer, Lengauer 2006; R Development Core Team 2007), allowing to handle other ontologies than the Gene Ontology. We defined the reference set as all the genes for which we had expression data in at least one structure of the organism across all life stages using *in-situ* hybridization data. This accounted for 9398 genes in zebrafish and 11322 genes in mouse, expressed in respectively 1067 and 2783 anatomical structures. Only anatomical structures with annotated expression of at least 5 genes were analyzed.

The expression data were propagated to parent structures in the ontology (e.g., a gene expressed in the “hindbrain” was also considered expressed in the parent structure “brain”), a methodology that is very helpful to automatically integrate large amounts of implicit knowledge. However this can result in the enrichment of non-independent terms, and of top-level terms of the ontology that are sometimes difficult to interpret, a behavior that is well known for Gene Ontology enrichment tests (Alexa, Rahnenfuhrer, Lengauer 2006; Falcon, Gentleman 2007; Yon Rhee et al. 2008). To correct for this effect, we used the “weight” algorithm available in the topGO package, a bottom-up approach that up or down-weights

terms depending on whether they benefit from the signal of their children structures (Alexa, Rahnenfuhrer, Lengauer 2006). Unless explicitly mentioned, this algorithm was used in the paper. Using another decorrelation algorithm of the topGO package, the "elim" algorithm, gave similar results (not shown).

A False Discovery Rate correction was applied on the list of *p*-values from tests on all anatomical structures. Structures enriched or depleted with a FDR < 10% are reported (Benjamini, Hochberg 1995). Of note, all analyses in this paper are reproducible using the TopAnat webservice available at http://bgee.org/?page=top_anat#/, as well as programmatically, using the BgeeDB Bioconductor package available at http://bioconductor.org/packages/release/bioc/html/BgeeDB.html. An example script is available as Supplementary material and on our GitHub repository (file expression_enrichment_with_BgeeDB.R). The results from the webservice and the Bioconductor package can differ slightly from our results due to slight differences on the handling of anatomical ontologies.

List of nervous system anatomical structures

A reference list of anatomical structures belonging to the nervous system in zebrafish and mouse was extracted from the Uberon ontology (as used in the Bgee database release 13). Because it was sometimes debatable whether a structure belonged to nervous system or not (e.g. sensory organs), we created a "strict" list and a "broad" list.

In zebrafish, the strict list included the "nervous system" structure (UBERON:0001016), as well as its sub-structures in the ontology. The "sensory system" structure (UBERON:0001032) and its sub-structures were removed. The broad list included them, as well as presumptive neural structures during development and their sub-structures (future nervous system, UBERON:0016880; neurectoderm, UBERON:0002346) and the structure "neurovascular bundle" and its sub-structures (UBERON:0016630).

In mouse, we used the same criteria, but we also noticed that some structures added to Uberon from the mouse-specific ontologies (EMAPA and MA ontologies) were not connected to any nervous system Uberon term at time of study. We thus added the following list of structures and their sub-structures to our broad list: nerves of urethra (EMAPA:31569), head or neck nerve or ganglion (MA:0000572 and MA:0000580), nerve of prostatic urethra (EMAPA:32279), nerves of urogenital sinus (EMAPA:31533), tail nervous system (EMAPA:16753), testicular branch of genital nerve (EMAPA:29731), nerve of prostate gland (EMAPA:32285), renal cortical nerves (EMAPA:31319), renal medullary nerves

(EMAPA:31354), nerve of bladder (EMAPA:31526), nerve of pelvic urethra (EMAPA:31558), and nerve of caudal urethra (EMAPA:31557). Note that many of these species-specific structures are connected to Uberon nervous system structures in the most recent release of Uberon.

The reference lists of nervous system structures were intersected with the list of anatomical structures showing expression of at least 5 genes, to keep only structures for which expression enrichment was effectively tested.

List of anatomical structures from other systems

We selected the high-level terms in the ontologies corresponding to these broad anatomical systems on zebrafish and mouse: Biliary system (UBERON:0002294), Circulatory system (UBERON:0001009), Digestive system (UBERON:0001007), Exocrine system (UBERON:0002330), Hematopoietic system (UBERON:0002390), Immune system (UBERON:0002405), Musculoskeletal (system UBERON:0002204), Renal system (UBERON:0001008), Reproductive system (UBERON:0000990), Respiratory system (UBERON:0001004) and Skeletal system (UBERON:0001434). We then retrieved all the sub-structures under these high-level terms down to the leaves of the ontology. We randomly picked five terms of the final lists of structures to verify manually that they indeed corresponded to the appropriate anatomical systems. We did not find any false positives during this process.

Similarly to the lists of nervous system structures, we retained in these lists only anatomical structures showing expression of at least 5 genes.

Rate of sequence evolution

We retrieved the rate of non-synonymous substitutions d_N and the rate of synonymous substitutions d_S for mouse genes from Ensembl release 79 (Hubbard et al. 2009) using BioMart (Smedley et al. 2009). The d_N and d_S values were calculated pairwise using one-to-one orthologs in rat (see http://www.ensembl.org/info/genome/compara/homology_method.html#dnds).

Gene Ontology

We retrieved genes annotated to the Gene Ontology category "metabolic process" (GO:0008152) and its sub-categories from the UniProtKB/Swiss-Prot database (The UniProt Consortium 2015), using the following URL:

http://www.uniprot.org/uniprot/?query=reviewed:yes+organism:%22Mus%20musculus%20(Mouse)%20[10090]%22+go:8152 (queried on Aug 2nd, 2016). We performed a similar query to retrieve genes annotated to the category "membrane" (GO:0016020; Supplementary Text).

Protein complexes

We obtained the precise annotation of number of subunits in protein complexes from manually curated information in the UniprotKB/Swiss-Prot database (The UniProt Consortium 2015). We downloaded data on July 21st, 2016 using the following URL: http://ebi4.uniprot.org/uniprot/?sort=&desc=&compress=no&query=&fil=reviewed:yes AND organism:"Mus musculus (Mouse) [10090]"&force=no&preview=true&format=tab&columns=id,genes,comment(SUBUNIT). We used regular expressions in a Perl script (available on our GitHub repository) to extract the free-text annotation about involvement in protein complexes in the "SUBUNIT" annotation field. We divided genes into the following categories: monomers (524 genes), homo-multimers (1,936 genes), hetero-dimers (746 genes), hetero-multimers with more than two subunits (e.g., hetero-trimers; 327 genes), and all other complexes that are not described precisely enough to be classified automatically (1,075 genes). The lists of genes in the different categories are available as supplementary material (file mouse_complexes.zip). If a gene was annotated in multiple categories, we kept it only in the "highest" category, following this order: hetero-multimer > hetero-dimer > uncharacterized complexes > homo-multimers > monomers.

Connectivity

We retrieved the numbers of direct neighbors of genes in the mouse protein-protein interactions network from the OGEE database. We downloaded the file connectivity.txt.gz at this link: http://ogeedb.embl.de/#download, on July 7th, 2016.

Akashi's test

Selection for translational accuracy was tested using Akashi's test (Akashi 1994; Drummond, Wilke 2008), following the procedure described at http://drummond.openwetware.org/Akashi's_Test.html. Alignments of mouse and rat protein-coding genes were retrieved from Ensembl using the Perl API. Sites with the same amino acid at the aligned position in mouse and rat sequences were designated conserved. Optimal codons in mouse were taken from Drummond and Wilke (Drummond, Wilke 2008). Laplace

smoothing was applied to contingency tables in order to remove problems with counts of zero. The outputs of the test are: (i) a *Z* score, which assesses how likely the association in a gene sequence between conserved sites and preferred codons is to have occurred by chance (significance), and (ii) a *Psi* score that assesses how strong is the association between preferred codons and conserved sites, which is computed as an odds ratio.

Translation rates

We downloaded the mean of the typical decoding rates (MTDR) index for mouse genes in embryonic stem cells, embryonic fibroblasts and neutrophils from http://www.cs.tau.ac.il/~tamirtul/MTDR/MTDR_ORF_values/ (Dana, Tuller 2014). The MTDR index represents the geometrical mean of the typical nominal translation rates of codons of a gene, estimated from ribosome profiling data, after filtering biases and the effects of phenomena such as ribosomal traffic jams and translational pauses.

False discovery rates

A false discovery rate of 10% was used to reported anatomical structures showing expression enrichment. For following analyses, where we disentangle the multiple factors associated with duplicate retention rates, we did not find a convenient way to correct for multiple testing. When enough independent tests of similar nature are performed, it is possible to estimate false discovery rates, but all our tests are not independent. Nonetheless, to give a rough estimate of the false discovery rate in these analyses, we collected all *p*-values generated for the linear regressions of the bin analyses in this paper (51 *p*-values). There was a clear excess of small *p*-values among them, indicating the presence of genuine signal (Figure S14). Using this list of *p*-values, we estimated that at a *p*-value threshold of 5%, the false discovery rate was well-controlled, at 10.2% using the FDR method (Benjamini, Hochberg 1995), or 3.4% using the q-value method (Storey, Tibshirani 2003).

Acknowledgements

We thank Frederic Bastian for help with Bgee data retrieval; members of the Robinson-Rechavi lab, Allan Drummond and Aoife McLysaght for helpful discussions; Adrian Alexa for help in the adaptation of the topGO package, and the ZFIN and GXD teams for providing *in situ* hybridization data and help with data retrieval. Part of the computations were performed at the Vital-IT (http://www.vital-it.ch) Center for high-performance computing of the SIB Swiss Institute of Bioinformatics. We acknowledge funding from Etat de Vaud and

Swiss National Science Foundation grant 31003A_153341 to MRR, Marie Curie IOF 273290 to JR, and Swiss Institute of Bioinformatics for support of the Bgee database.

Author contributions

JR made the original observation; JR and JL designed the detailed study with input from MRR; JR and JL analyzed the data; JR wrote the paper with input from JL and MRR.

Tables

Table 1:

Zebrafish anatomical structures showing a significant enrichment in expression of zebrafish 3R ohnologs (FDR < 10%). Anatomical structures are sorted by their enrichment fold compared to null expectation. The sub-structures of the "broad" nervous system are highlighted in bold. The "weight" algorithm of the topGO package was used to decorrelate the structure of the ontology. The full list of anatomical structures, sorted by *p*-value, is shown in Table S1.

Organ ID	Organ name	Number of genes expressed	Number of 3R ohnologs expressed	Number of 3R ohnologs expected	Enrichment fold	*p*-value	FDR
UBERON:2007001	**dorso-rostral cluster**	18	9	1.88	4.79	2.91E-05	3.02E-03
UBERON:2007002	**ventro-rostral cluster**	21	10	2.19	4.57	1.78E-05	2.00E-03
UBERON:2007003	**ventro-caudal cluster**	19	9	1.99	4.52	5.01E-05	4.23E-03
UBERON:0000204	**ventral part of telencephalon**	102	25	10.66	2.35	3.48E-05	3.36E-03
UBERON:0002946	**regional part of cerebellum**	79	19	8.26	2.30	3.86E-04	2.74E-02
UBERON:0002757	**regional part of epithalamus**	546	121	57.06	2.12	1.30E-16	8.78E-14
UBERON:0008904	**neuromast**	169	37	17.66	2.10	8.91E-06	1.09E-03
UBERON:0000203	**pallium**	105	23	10.97	2.10	4.27E-04	2.88E-02
UBERON:0003895	hypaxial myotome region	101	22	10.55	2.09	6.13E-04	3.76E-02
UBERON:0010134	**secretory circumventricular organ**	478	104	49.95	2.08	8.10E-14	3.64E-11
UBERON:0003902	**retinal neural layer**	633	136	66.15	2.06	2.09E-17	2.82E-14
UBERON:0003296	**gland of diencephalon**	559	115	58.42	1.97	1.70E-13	5.73E-11
UBERON:0002540	**lateral line system**	519	101	54.24	1.86	6.78E-06	9.15E-04
UBERON:0001898	**hypothalamus**	329	59	34.38	1.72	6.10E-04	3.76E-02
UBERON:0000045	**ganglion**	596	105	62.28	1.69	2.26E-08	5.07E-06
UBERON:0002199	integument	565	97	59.04	1.64	3.51E-07	5.92E-05
UBERON:0001894	**diencephalon**	1459	239	152.47	1.57	1.82E-03	9.82E-02
UBERON:0005725	**olfactory system**	760	124	79.42	1.56	6.94E-08	1.34E-05
UBERON:0002298	**brainstem**	624	101	65.21	1.55	3.79E-05	3.41E-03
UBERON:0003051	ear vesicle	843	133	88.09	1.51	9.98E-07	1.50E-04
UBERON:0000489	cavitated compound organ	1701	255	177.76	1.43	1.34E-08	3.63E-06
UBERON:0002028	**hindbrain**	1600	225	167.2	1.35	7.71E-05	6.11E-03
UBERON:0000479	tissue	4751	645	496.49	1.30	1.29E-03	7.27E-02
UBERON:0000955	**brain**	3255	435	340.15	1.28	1.29E-04	9.70E-03
UBERON:0000483	epithelium	3734	489	390.21	1.25	8.56E-04	5.02E-02

Figures legends

Figure 1: Proportion of mouse orthologs of zebrafish 3R ohnologs among genes expressed in the different tissues sampled in the GSE3594 microarray experiment. The reference gene set was composed only of mouse orthologs of zebrafish 3R ohnologs and singletons. Tissues are ranked based on the average proportion of orthologs of ohnologs expressed. Each dot represents a sample (biological replicate). Green color represents nervous-system tissues and purple represents non-nervous-system tissues.

Figure 2:

A: Comparison of the rate of protein sequence evolution (d_N, plotted in $\log_{10}$ scale) for mouse orthologs of zebrafish 3R ohnologs ("Dup.") or singletons ("Sing."). The number of genes in each category is indicated below each box. The *p*-values from a Wilcoxon test comparing categories are reported above boxes.

B: similar to (A), but mouse orthologs of zebrafish 3R ohnologs and singletons are split according to their expression in the nervous system ("Nervous system" and "Non-nervous system"). The numbers of duplicates and singletons genes do not add up to numbers of genes in (A) because only genes with *in situ* hybridization data were used for this analysis.

Figure 3:

A: Relation between proportion of mouse orthologs of zebrafish 3R ohnologs and rate of non-synonymous substitution. Genes were split into 10 equal-sized bins of d_N, and the median d_N of each bin was plotted on the x-axis (in $\log_{10}$ scale). A linear regression was fit to the 10 data points, whose slope (Beta value) and *p*-value are indicated in the top-right corner of the plot. The analysis including all genes is plotted in grey and circles, while the analysis including only nervous system genes is plotted in green and squares and the analysis including only non-nervous system genes is plotted in purple and triangles.

B: Relation between proportion of mouse orthologs of zebrafish 3R ohnologs and Akashi's test *Psi* score, for nervous and non-nervous system genes. Legend similar to (A).

C: Similar to (A), using only nervous system genes, divided in two groups: the 20% genes with lowest *Psi* score plotted in blue and squares, and the 20% genes with highest *Psi* score plotted in red and triangles.

D: Similar to (B), using only nervous system genes, divided in two groups: the 20% genes with lowest d_N plotted in blue and squares, and the 20% genes with highest d_N plotted in red and triangles.

Figure 4:
Illustration of the model proposed to explain favored retention of nervous system genes after whole-genome duplication. Non-synonymous mutations or synonymous mutations at structurally sensitive sites on one duplicate copy can cause an increase in the production of non-functional misfolded proteins. This is likely neutral in most tissues, since the function loss is backed-up by the other copy. This is however likely deleterious for nervous system genes because non-renewing nervous tissues are sensitive to the aggregation of misfolded proteins. Purifying selection will thus prevent the fixation of such mutations, and indirectly contribute to the preservation of both ohnologs.

Supplementary figures

Figure S1:
Illustration of the tree topologies targeted in this paper to identify duplicate and singleton genes. See "identification of duplicates and singletons" in the Materials and Methods for explanations complementing this figure. Black circles represent speciation nodes and red squares duplication nodes. Lineages in dotted lines represent lineages that were allowed in the selected topologies, but could be absent in some trees. Lineages names in red represent the target species (zebrafish or mouse). Internal node annotations represent the targeted taxonomical levels.
A: 3R ohnologs in zebrafish.
B: 3R singletons in zebrafish.
C: mouse orthologs of zebrafish 3R ohnologs.
D: mouse orthologs of zebrafish 3R singletons.
E: 2R ohnologs in mouse
F: 2R singletons in mouse
G: Small-scale duplicates in zebrafish. Paralogs with 100% or <10% sequence identity were filtered out.
H: Small-scale duplicates in mouse. Paralogs with 100% or <10% sequence identity were filtered out.

Figure S2:

(A) Proportion of mouse orthologs of zebrafish 3R ohnologs among genes expressed in the different tissues sampled in the GSE10246 microarray experiment. Legend as Figure 1.

(B) Boxplot of the proportion of human orthologs of zebrafish 3R ohnologs among genes expressed in the different tissues sampled in the GTEx RNA-seq experiment.

(C) Proportion of mouse orthologs of zebrafish 3R ohnologs among genes expressed in the different tissues sampled in the GSE16496 microarray experiment.

Figure S3:

A: Spearman's correlation coefficient between d_N and the expression levels in the different tissues sampled in the GSE3594 microarray experiment. Tissues are ranked based on the average correlation coefficient across biological replicates, represented with different dots. Green color represents nervous-system tissues and purple represents non-nervous-system tissues. "Mean expression" and "maximum expression" represent the correlation between d_N and the mean or maximum expression levels across all samples. "Mean nervous system expression" and "maximum nervous system expression" represent the correlation between d_N and the mean or maximum expression levels across all samples from nervous system tissues.

B: Similar to (A), but using samples from the GSE16496 microarray experiment including only nervous tissues. "Mean nervous system expression*" and "maximum nervous system expression*" represent the correlation between d_N and the mean or maximum expression levels across all samples from nervous system tissues, excluding samples from the three nervous tissues displaying lower correlation than other: retina, pineal body and pituitary gland.

Figure S4:

Scatterplots illustrating, in mouse, the pairwise relationships between the gene properties used in this paper. Spearman's correlation coefficients (rho) and *p*-values are indicated in the top-right corner of the figures. Loess regression lines are plotted in red.

A: relation between d_N and mean expression level across nervous system samples from the GSE16496 microarray experiment.

B: relation between d_N and maximum expression level across nervous system samples from the GSE16496 microarray experiment.

C: relation between d_N and d_S.

D: relation between d_S and maximum nervous system expression level.

E: relation between d_N and Akashi's test *Psi* score.

F: relation between *Psi* and maximum nervous system expression level.

G: relation between d_N and connectivity (number of protein-protein interactions).

H: relation between *Psi* and connectivity.

I: relation between connectivity and maximum nervous system expression level.

Figure S5:

A: Relation between proportion of mouse orthologs of zebrafish 3R ohnologs and expression levels summaries, mean and maximum nervous system expression. Only nervous system genes were used for this analysis. Genes were split into 10 equal-sized bins of expression levels, and the median expression level of each bin was plotted on the x-axis (in $\log_2$ scale). The analysis using mean nervous system expression is plotted in dashed line and open circles, while the analysis using maximum nervous system expression is plotted in solid line and plain circles.

B: Similar to A, using maximum nervous system expression. The analysis including the 20% genes with highest d_N is plotted in blue and squares, while the analysis including 20% genes with lowest d_N is plotted in red and triangles.

C: Similar to Figure 3C. The analysis including the 20% genes with highest maximum nervous system expression is plotted in red and squares, while the analysis including the 20% genes with lowest maximum nervous system expression is plotted in blue and triangles.

Figure S6:

A: Spearman's correlation coefficient between d_S and the expression levels in the different tissues sampled in the GSE3594 microarray experiment. Legend similar to Figure S3.

B: Relation between proportion of mouse orthologs of zebrafish 3R ohnologs and rate of synonymous substitution. Legend similar to Figure 3A and B.

Figure S7:

Relation between Akashi's test *Psi* score and translation rates across three different cell types in mouse. Legend similar to Figure S4.

A: neutrophils

B: embryonic fibroblasts

C: embryonic stem cells

Figure S8:

A: Proportion of mouse orthologs of zebrafish 3R ohnologs for members of different complexes subtypes, classified using UniProtKB/Swiss-Prot data. The number of genes in each category is indicated at the bottom of each box. Green bars represent nervous system genes and purple bars represent non-nervous system genes.

B: Relation between proportion of mouse orthologs of zebrafish 3R ohnologs and d_N, controlling for complex membership. Legend similar to Figure 3C. Genes were divided into different groups based on their membership in protein complexes, using data from the UniProtKB/Swiss-Prot database.

Figure S9:

Proportion of mouse orthologs of zebrafish 3R ohnologs for metabolic process and non-metabolic process genes, based on Gene Ontology annotation. Legend similar to Figure S8A.

Figure S10:

A: Comparison of connectivity for mouse orthologs of zebrafish 3R ohnologs or singletons, depending on their nervous system expression. Legend similar to Figure 2.

B: Relation between proportion of mouse orthologs of zebrafish 3R ohnologs and d_N, controlling for connectivity. Legend similar to Figure 3.

C: Relation between proportion of mouse orthologs of zebrafish 3R ohnologs and connectivity, controlling for d_N. Legend similar to Figure 3.

D: Relation between proportion of mouse orthologs of zebrafish 3R ohnologs and connectivity, controlling for complex membership. Legend similar to Figure S8B.

Figure S11: Relation between the proportion of small-scale duplicates in mouse, and nervous system expression, d_N, and *Psi* score.

A: Similar as Figure 2.

B and C: Similar to Figure 3C and D, but including all genes.

Figure S12:

A: Relation between proportion of mouse small-scale duplicates and expression levels summaries, mean and maximum expression across all samples from the GSE3594 microarray experiment. Legend similar to Figure S5A. The analysis using mean expression is plotted in

plain line and plain circles, while the analysis using maximum expression is plotted in dashed line and open circles.
B and C: Similar to Figure S5B and C for mouse small-scale duplicates, using mean expression level.

Figure S13:
Proportion of mouse small-scale duplicates for members of different complexes subtypes. Legend similar to Figure S8.

Figure S14:
Histogram of *p*-values from 51 linear regressions performed in Figures 3, S5, S6, S8, S10, S11, S12 and S16. A dashed red line indicates the 5% significance threshold used in this study.

Figure S15 (Supplementary Text):
Histogram of *p*-values from 10,000 Wilcoxon tests obtained by comparing the d_N values of nervous system orthologs of ohnologs and singletons, after randomly resampling the set of nervous system genes to the same size as the set of non-nervous system genes. A dashed red line indicates p=0.05, and a plain red line indicates p=0.41 (the p-value obtained from the Wilcoxon test between non-nervous system orthologs of ohnologs and singletons, see Figure 2B).

Figure S16 (Supplementary Text):
A: Proportion of mouse orthologs of zebrafish 3R ohnologs for members of different complexes subtypes, classified using data from the CORUM database. Similar to Figure S8.
B: Proportion of mouse small-scale duplicates for members of different complexes subtypes. Similar to Figure S13.

Figure S17 (Supplementary Text):
A: Proportion of mouse orthologs of zebrafish 3R ohnologs for genes encoding membrane proteins or not, based on Gene Ontology annotation. Legend similar to Figure S8A.
B: Relation between proportion of mouse orthologs of zebrafish 3R ohnologs and d_N, controlling for the effect of encoding a membrane protein. Legend similar to Figure 3.

Supplementary tables

Table S1:

Zebrafish anatomical structures showing a significant enrichment in expression of zebrafish 3R ohnologs. Similar to Table 1, but all structures are shown, even non-significant ones.

Table S2: Zebrafish anatomical structures showing a significant depletion in expression of 3R singletons.

Table S3: Same as Table S1 but using an independent list of zebrafish 3R ohnologs obtained from (Braasch et al. 2016).

Table S4: Same as Table S2 but using an independent list of zebrafish 3R singletons obtained from (Braasch et al. 2016).

Table S5: Mouse anatomical structures showing a significant enrichment in expression of orthologs of zebrafish 3R ohnologs.

Table S6: Mouse anatomical structures showing a depletion in expression of orthologs of zebrafish 3R singletons.

Table S7: Mouse anatomical structures showing a significant enrichment in expression of 2R ohnologs.

Table S8: Same as Table S7 but using an independent list of mouse 2R ohnologs obtained from (Singh, Arora, Isambert 2015). The three lists of 2R ohnologs, calculated with different levels of stringency are available at http://ohnologs.curie.fr/cgi-bin/BrowsePage.cgi?org=mouse. Here, the most stringent list was used, but the results were similar with the intermediate and relaxed lists.

Table S9: Mouse anatomical structures showing a significant depletion in expression of 2R singletons.

Table S10: Mouse anatomical structures showing a significant depletion in expression of small-scale duplicates.

Table S11: Same as Table S10 but using an independent list of rodent-specific small-duplicate genes obtained from (Farre, Alba 2010).

Table S12: Mouse anatomical structures showing a significant enrichment in expression of slowly evolving genes (the 10% lowest d_N values based on mouse-rat comparisons; FDR < 10%).

Table S13: Mouse anatomical structures showing a significant enrichment in expression of genes with the 10% highest *Psi* score from Akashi's test.

References

Akashi H. 1994. Synonymous codon usage in Drosophila melanogaster: natural selection and translational accuracy. Genetics 136:927-935.

Albalat R, Canestro C. 2016. Evolution by gene loss. Nat Rev Genet 17:379-391.

Alexa A, Rahnenfuhrer J, Lengauer T. 2006. Improved scoring of functional groups from gene expression data by decorrelating GO graph structure. Bioinformatics 22:1600-1607.

Altschuler SJ, Wu LF. 2010. Cellular heterogeneity: do differences make a difference? Cell 141:559-563.

Ashburner M, Ball CA, Blake JA, et al. 2000. Gene ontology: tool for the unification of biology. The Gene Ontology Consortium. Nat Genet 25:25-29.

Aury JM, Jaillon O, Duret L, et al. 2006. Global trends of whole-genome duplications revealed by the ciliate Paramecium tetraurelia. Nature 444:171-178.

Barbosa-Morais NL, Irimia M, Pan Q, et al. 2012. The evolutionary landscape of alternative splicing in vertebrate species. Science 338:1587-1593.

Bard JBL, Kaufman MH, Dubreuil C, Brune RM, Burger A, Baldock RA, Davidson DR. 1998. An internet-accessible database of mouse developmental anatomy based on a systematic nomenclature. Mech Dev 74:111-120.

Bastian F, Parmentier G, Roux J, Moretti S, Laudet V, Robinson-Rechavi M. 2008. Bgee: Integrating and Comparing Heterogeneous Transcriptome Data Among Species. DILS: Data Integration in the Life Sciences. p. 124-131.

Bekaert M, Edger PP, Pires JC, Conant GC. 2011. Two-phase resolution of polyploidy in the Arabidopsis metabolic network gives rise to relative and absolute dosage constraints. Plant Cell 23:1719-1728.

Benjamini Y, Hochberg Y. 1995. Controlling the False Discovery Rate: A Practical and Powerful Approach to Multiple Testing. Journal of the Royal Statistical Society. Series B (Methodological) 57:289-300.

Birchler JA, Veitia RA. 2012. Gene balance hypothesis: connecting issues of dosage sensitivity across biological disciplines. Proc Natl Acad Sci U S A 109:14746-14753.

Biswas K, Chakraborty S, Podder S, Ghosh TC. 2016. Insights into the dN/dS ratio heterogeneity between brain specific genes and widely expressed genes in species of different complexity. Genomics 108:11-17.
Braasch I, Gehrke AR, Smith JJ, et al. 2016. The spotted gar genome illuminates vertebrate evolution and facilitates human-teleost comparisons. Nat Genet 48:427-437.
Brawand D, Soumillon M, Necsulea A, et al. 2011. The evolution of gene expression levels in mammalian organs. Nature 478:343-348.
Bray NL, Pimentel H, Melsted P, Pachter L. 2016. Near-optimal probabilistic RNA-seq quantification. Nat Biotechnol.
Brunet FG, Crollius HR, Paris M, Aury JM, Gibert P, Jaillon O, Laudet V, Robinson-Rechavi M. 2006. Gene loss and evolutionary rates following whole-genome duplication in teleost fishes. Mol Biol Evol 23:1808-1816.
Chakraborty M, Jarvis ED. 2015. Brain evolution by brain pathway duplication. Philos Trans R Soc Lond B Biol Sci 370:20150056.
Chen W-H, Zhao X-M, van Noort V, Bork P. 2013. Human Monogenic Disease Genes Have Frequently Functionally Redundant Paralogs. PLoS Comput Biol 9:e1003073.
Chen Y, Ding Y, Zhang Z, Wang W, Chen JY, Ueno N, Mao B. 2011. Evolution of vertebrate central nervous system is accompanied by novel expression changes of duplicate genes. J Genet Genomics 38:577-584.
Conant GC, Wolfe KH. 2008. Turning a hobby into a job: How duplicated genes find new functions. Nat Rev Genet 9:938-950.
Cuypers TD, Hogeweg P. 2014. A Synergism between Adaptive Effects and Evolvability Drives Whole Genome Duplication to Fixation. PLoS Comput Biol 10:e1003547.
Dana A, Tuller T. 2014. Mean of the typical decoding rates: a new translation efficiency index based on the analysis of ribosome profiling data. G3 (Bethesda) 5:73-80.
Davis JC, Petrov DA. 2004. Preferential duplication of conserved proteins in eukaryotic genomes. PLoS Biol 2:e55.
Davis JC, Petrov DA. 2005. Do disparate mechanisms of duplication add similar genes to the genome? Trends Genet 21:548-551.
Dickerson JE, Robertson DL. 2012. On the origins of Mendelian disease genes in man: the impact of gene duplication. Mol Biol Evol 29:61-69.
Diez-Roux G, Banfi S, Sultan M, et al. 2011. A High-Resolution Anatomical Atlas of the Transcriptome in the Mouse Embryo. PLoS Biol 9:e1000582.
Drummond DA, Bloom JD, Adami C, Wilke CO, Arnold FH. 2005. Why highly expressed proteins evolve slowly. Proc Natl Acad Sci U S A 102:14338-14343.
Drummond DA, Raval A, Wilke CO. 2006. A single determinant dominates the rate of yeast protein evolution. Mol Biol Evol 23:327-337.
Drummond DA, Wilke CO. 2008. Mistranslation-Induced Protein Misfolding as a Dominant Constraint on Coding-Sequence Evolution. Cell 134:341-352.
Drummond DA, Wilke CO. 2009. The evolutionary consequences of erroneous protein synthesis. Nat Rev Genet 10:715-724.
Duret L, Mouchiroud D. 2000. Determinants of Substitution Rates in Mammalian Genes: Expression Pattern Affects Selection Intensity but Not Mutation Rate. Mol Biol Evol 17:68-70.
Evlampiev K, Isambert H. 2007. Modeling protein network evolution under genome duplication and domain shuffling. BMC Systems Biology 1:1-18.
Falcon S, Gentleman R. 2007. Using GOstats to test gene lists for GO term association. Bioinformatics 23:257-258.

Fares MA, Keane OM, Toft C, Carretero-Paulet L, Jones GW. 2013. The roles of whole-genome and small-scale duplications in the functional specialization of Saccharomyces cerevisiae genes. PLoS Genet 9:e1003176.
Farre D, Alba MM. 2010. Heterogeneous Patterns of Gene-Expression Diversification in Mammalian Gene Duplicates. Mol Biol Evol 27:325-335.
Flagel LE, Wendel JF. 2009. Gene duplication and evolutionary novelty in plants. New Phytol 183:557-564.
Force A, Lynch M, Pickett FB, Amores A, Yan YL, Postlethwait J. 1999. Preservation of duplicate genes by complementary, degenerative mutations. Genetics 151:1531-1545.
Freeling M, Thomas BC. 2006. Gene-balanced duplications, like tetraploidy, provide predictable drive to increase morphological complexity. Genome Res 16:805-814.
Gentleman R, Carey V, Bates D, et al. 2004. Bioconductor: open software development for computational biology and bioinformatics. Genome Biol 5:R80.
Gibson TJ, Spring J. 1998. Genetic redundancy in vertebrates: polyploidy and persistence of genes encoding multidomain proteins. Trends Genet 14:46-49.
Gould SJ, Lewontin RC. 1979. The spandrels of San Marco and the Panglossian paradigm: a critique of the adaptationist programme. Proc R Soc B 205:581-598.
Gout J-F, Duret L, Kahn D. 2009. Differential Retention of Metabolic Genes Following Whole-Genome Duplication. Mol Biol Evol 26:1067-1072.
Gout J-F, Kahn D, Duret L, Paramecium Post-Genomics C. 2010. The Relationship among Gene Expression, the Evolution of Gene Dosage, and the Rate of Protein Evolution. PLoS Genet 6:e1000944.
Gout J-F, Lynch M. 2015. Maintenance and Loss of Duplicated Genes by Dosage Subfunctionalization. Mol Biol Evol 32:2141-2148.
Gu X, Su Z. 2007. Tissue-driven hypothesis of genomic evolution and sequence-expression correlations. Proc Natl Acad Sci U S A 104:2779-2784.
Haendel MA, Balhoff JP, Bastian FB, et al. 2014. Unification of multi-species vertebrate anatomy ontologies for comparative biology in Uberon. J Biomed Semantics 5:21.
Hakes L, Pinney JW, Lovell SC, Oliver SG, Robertson DL. 2007. All duplicates are not equal: the difference between small-scale and genome duplication. Genome Biol 8:R209.
Hayamizu TF, Mangan M, Corradi JP, Kadin JA, Ringwald M. 2005. The Adult Mouse Anatomical Dictionary: a tool for annotating and integrating data. Genome Biol 6:R29.
Hayamizu TF, Wicks MN, Davidson DR, Burger A, Ringwald M, Baldock RA. 2013. EMAP/EMAPA ontology of mouse developmental anatomy: 2013 update. J Biomed Semantics 4:15.
He X, Zhang J. 2005. Rapid Subfunctionalization Accompanied by Prolonged and Substantial Neofunctionalization in Duplicate Gene Evolution. Genetics 169:1157-1164.
Holland LZ. 2009. Chordate roots of the vertebrate nervous system: expanding the molecular toolkit. Nat Rev Neurosci 10:736-746.
Holland PWH, Garcia-Fernàndez J, Williams NA, Sidow A. 1994. Gene duplications and the origins of vertebrate development. Development 1994:125-133.
Howe K, Clark MD, Torroja CF, et al. 2013. The zebrafish reference genome sequence and its relationship to the human genome. Nature 496:498-503.
Hubbard TJ, Aken BL, Ayling S, et al. 2009. Ensembl 2009. Nucleic Acids Res 37:D690-697.
Hughes AL. 1999. Phylogenies of Developmentally Important Proteins Do Not Support the Hypothesis of Two Rounds of Genome Duplication Early in Vertebrate History. Journal of Molecular Evolution 48:565-576.

Huminiecki L, Heldin CH. 2010. 2R and remodeling of vertebrate signal transduction engine. BMC Biology 8:1-21.
Innan H, Kondrashov F. 2010. The evolution of gene duplications: classifying and distinguishing between models. Nat Rev Genet 11:97-108.
Jacobs NL, Albertson RC, Wiles JR. 2011. Using Whole Mount in situ Hybridization to Link Molecular and Organismal Biology. J. Vis. Exp.:e2533.
Jaillon O, Aury J-M, Brunet F, et al. 2004. Genome duplication in the teleost fish Tetraodon nigroviridis reveals the early vertebrate proto-karyotype. Nature 431:946-957.
Jordan IK, Wolf YI, Koonin EV. 2004. Duplicated genes evolve slower than singletons despite the initial rate increase. BMC Evol Biol 4:22.
Kassahn KS, Dang VT, Wilkins SJ, Perkins AC, Ragan MA. 2009. Evolution of gene function and regulatory control after whole-genome duplication: Comparative analyses in vertebrates. Genome Res 19:1404-1418.
Kasukawa T, Masumoto KH, Nikaido I, Nagano M, Uno KD, Tsujino K, Hanashima C, Shigeyoshi Y, Ueda HR. 2011. Quantitative expression profile of distinct functional regions in the adult mouse brain. PLoS ONE 6:e23228.
Kondrashov FA. 2012. Gene duplication as a mechanism of genomic adaptation to a changing environment. Proc Biol Sci 279:5048-5057.
Kryuchkova-Mostacci N, Robinson-Rechavi M. 2015. Tissue-Specific Evolution of Protein Coding Genes in Human and Mouse. PLoS ONE 10:e0131673.
Lan X, Pritchard JK. 2016. Coregulation of tandem duplicate genes slows evolution of subfunctionalization in mammals. Science 352:1009-1013.
Lein ES, Hawrylycz MJ, Ao N, et al. 2007. Genome-wide atlas of gene expression in the adult mouse brain. Nature 445:168-176.
Liang H, Li WH. 2007. Gene essentiality, gene duplicability and protein connectivity in human and mouse. Trends Genet 23:375-378.
Liu WM, Mei R, Di X, et al. 2002. Analysis of high density expression microarrays with signed-rank call algorithms. Bioinformatics 18:1593-1599.
Lynch M, Conery JS. 2000. The Evolutionary Fate and Consequences of Duplicate Genes. Science 290:1151-1155.
Makino T, Hokamp K, McLysaght A. 2009. The complex relationship of gene duplication and essentiality. Trends Genet 25:152-155
Makino T, McLysaght A. 2010. Ohnologs in the human genome are dosage balanced and frequently associated with disease. Proc Natl Acad Sci U S A 107:9270-9274.
Malaguti G, Singh PP, Isambert H. 2014. On the retention of gene duplicates prone to dominant deleterious mutations. Theor Popul Biol 93:38-51.
McLysaght A, Makino T, Grayton HM, Tropeano M, Mitchell KJ, Vassos E, Collier DA. 2014. Ohnologs are overrepresented in pathogenic copy number mutations. Proc Natl Acad Sci U S A 111:361-366.
Melé M, Ferreira PG, Reverter F, et al. 2015. The human transcriptome across tissues and individuals. Science 348:660-665.
Merkin J, Russell C, Chen P, Burge CB. 2012. Evolutionary dynamics of gene and isoform regulation in Mammalian tissues. Science 338:1593-1599.
Meyer A, Van de Peer Y. 2005. From 2R to 3R: evidence for a fish-specific genome duplication (FSGD). BioEssays 27:937-945.
Mungall CJ, Torniai C, Gkoutos GV, Lewis SE, Haendel MA. 2012. Uberon, an integrative multi-species anatomy ontology. Genome Biol 13:R5.
Musso G, Zhang Z, Emili A. 2007. Retention of protein complex membership by ancient duplicated gene products in budding yeast. Trends Genet 23:266-269.

Nakatani Y, Takeda H, Kohara Y, Morishita S. 2007. Reconstruction of the vertebrate ancestral genome reveals dynamic genome reorganization in early vertebrates. Genome Res 17:1254-1265.
Neidhardt L, Gasca S, Wertz K, Obermayr F, Worpenberg S, Lehrach H, Herrmann BG. 2000. Large-scale screen for genes controlling mammalian embryogenesis, using high-throughput gene expression analysis in mouse embryos. Mechanisms of Development 98:77-93.
Oakley TH, Rivera AS. 2008. Genomics and the evolutionary origins of nervous system complexity. Curr Opin Genet Dev 18:479-492.
Ohno S. 1970. Evolution by gene duplication: Springer-Verlag.
Osborn TC, Chris Pires J, Birchler JA, et al. 2003. Understanding mechanisms of novel gene expression in polyploids. Trends in Genetics 19:141-147.
Pantalacci S, Semon M. 2015. Transcriptomics of developing embryos and organs: A raising tool for evo-devo. J Exp Zool B Mol Dev Evol 324:363-371.
Papp B, Pal C, Hurst LD. 2003. Dosage sensitivity and the evolution of gene families in yeast. Nature 424:194-197.
Pegueroles C, Laurie S, Alba MM. 2013. Accelerated evolution after gene duplication: a time-dependent process affecting just one copy. Mol Biol Evol 30:1830-1842.
Pennacchio LA, Ahituv N, Moses AM, et al. 2006. In vivo enhancer analysis of human conserved non-coding sequences. Nature 444:499-502.
Prachumwat A, Li W-H. 2006. Protein Function, Connectivity, and Duplicability in Yeast. Mol Biol Evol 23:30-39.
Putnam NH, Butts T, Ferrier DEK, et al. 2008. The amphioxus genome and the evolution of the chordate karyotype. Nature 453:1064-1071.
Qian W, Zhang J. 2014. Genomic evidence for adaptation by gene duplication. Genome Res 24:1356-1362.
R Development Core Team. 2007. R: A Language and Environment for Statistical Computing. Vienna, Austria: R Foundation for Statistical Computing.
Rodgers-Melnick E, Culp M, DiFazio SP. 2013. Predicting whole genome protein interaction networks from primary sequence data in model and non-model organisms using ENTS. BMC Genomics 14:1-17.
Rodgers-Melnick E, Mane SP, Dharmawardhana P, Slavov GT, Crasta OR, Strauss SH, Brunner AM, Difazio SP. 2012. Contrasting patterns of evolution following whole genome versus tandem duplication events in Populus. Genome Res 22:95-105.
Roux J, Robinson-Rechavi M. 2008. Developmental Constraints on Vertebrate Genome Evolution. PLoS Genet 4:e1000311.
Satake M, Kawata M, McLysaght A, Makino T. 2012. Evolution of vertebrate tissues driven by differential modes of gene duplication. DNA Res 19:305-316.
Schartl M, Walter RB, Shen Y, et al. 2013. The genome of the platyfish, Xiphophorus maculatus, provides insights into evolutionary adaptation and several complex traits. Nat Genet 45:567-572.
Schuster EF, Blanc E, Partridge L, Thornton JM. 2007. Correcting for sequence biases in present/absent calls. Genome Biol 8:R125.
Schuster-Böckler B, Conrad D, Bateman A. 2010. Dosage Sensitivity Shapes the Evolution of Copy-Number Varied Regions. PLoS ONE 5:e9474.
Singh PP, Affeldt S, Cascone I, Selimoglu R, Camonis J, Isambert H. 2012. On the expansion of "dangerous" gene repertoires by whole-genome duplications in early vertebrates. Cell Rep 2:1387-1398.

Singh PP, Affeldt S, Malaguti G, Isambert H. 2014. Human Dominant Disease Genes Are Enriched in Paralogs Originating from Whole Genome Duplication. PLoS Comput Biol 10:e1003754.
Singh PP, Arora J, Isambert H. 2015. Identification of Ohnolog Genes Originating from Whole Genome Duplication in Early Vertebrates, Based on Synteny Comparison across Multiple Genomes. PLoS Comput Biol 11:e1004394.
Smedley D, Haider S, Ballester B, Holland R, London D, Thorisson G, Kasprzyk A. 2009. BioMart--biological queries made easy. BMC Genomics 10:22.
Smith CM, Finger JH, Hayamizu TF, McCright IJ, Eppig JT, Kadin JA, Richardson JE, Ringwald M. 2007. The mouse Gene Expression Database (GXD): 2007 update. Nucleic Acids Res 35:D618-623.
Smith CM, Finger JH, Hayamizu TF, et al. 2014. The mouse Gene Expression Database (GXD): 2014 update. Nucleic Acids Res 42:D818-824.
Smith JJ, Keinath MC. 2015. The sea lamprey meiotic map improves resolution of ancient vertebrate genome duplications. Genome Res 25:1081-1090.
Sprague J, Bayraktaroglu L, Clements D, et al. 2006. The Zebrafish Information Network: the zebrafish model organism database. Nucleic Acids Res 34:D581-585.
Storey JD, Tibshirani R. 2003. Statistical significance for genomewide studies. Proc Natl Acad Sci U S A 100:9440-9445.
Su AI, Wiltshire T, Batalov S, et al. 2004. A gene atlas of the mouse and human protein-encoding transcriptomes. Proc Natl Acad Sci U S A 101:6062-6067.
The GTEx Consortium. 2015. The Genotype-Tissue Expression (GTEx) pilot analysis: Multitissue gene regulation in humans. Science 348:648-660.
The UniProt Consortium. 2015. UniProt: a hub for protein information. Nucleic Acids Res 43:D204-212.
Thisse B, Heyer V, Lux A, Alunni V, Degrave A, Seiliez I, Kirchner J, Parkhill JP, Thisse C. 2004. Spatial and temporal expression of the zebrafish genome by large-scale in situ hybridization screening. Methods Cell Biol 77:505-519.
Thompson A, Zakon HH, Kirkpatrick M. 2016. Compensatory Drift and the Evolutionary Dynamics of Dosage-Sensitive Duplicate Genes. Genetics 202:765-774.
Tinti M, Dissanayake K, Synowsky S, Albergante L, MacKintosh C. 2014. Identification of 2R-ohnologue gene families displaying the same mutation-load skew in multiple cancers. Open Biol 4:140029.
Van de Peer Y, Maere S, Meyer A. 2009. The evolutionary significance of ancient genome duplications. Nat Rev Genet 10:725-732.
Vavouri T, Semple JI, Garcia-Verdugo R, Lehner B. 2009. Intrinsic protein disorder and interaction promiscuity are widely associated with dosage sensitivity. Cell 138:198-208.
Veitia RA, Bottani S, Birchler JA. 2008. Cellular reactions to gene dosage imbalance: genomic, transcriptomic and proteomic effects. Trends Genet 24:390-397.
Vilella AJ, Severin J, Ureta-Vidal A, Heng L, Durbin R, Birney E. 2009. EnsemblCompara GeneTrees: Complete, duplication-aware phylogenetic trees in vertebrates. Genome Res 19:327-335.
Wang G. 2016. Highly expressed proteins prefer less informative amino acids. bioRxiv.
Yang JR, Liao BY, Zhuang SM, Zhang J. 2012. Protein misinteraction avoidance causes highly expressed proteins to evolve slowly. Proc Natl Acad Sci U S A 109:E831-840.
Yang JR, Zhuang SM, Zhang J. 2010. Impact of translational error-induced and error-free misfolding on the rate of protein evolution. Mol Syst Biol 6:421.
Yon Rhee S, Wood V, Dolinski K, Draghici S. 2008. Use and misuse of the gene ontology annotations. Nat Rev Genet 9:509-515.

Zapala MA, Hovatta I, Ellison JA, et al. 2005. Adult mouse brain gene expression patterns bear an embryologic imprint. Proc Natl Acad Sci U S A 102:10357-10362.
Zhang J, Maslov S, Shakhnovich EI. 2008. Constraints imposed by non-functional protein-protein interactions on gene expression and proteome size. Mol Syst Biol 4:210.
Zhang J, Yang JR. 2015. Determinants of the rate of protein sequence evolution. Nat Rev Genet 16:409-420.
Zhou T, Weems M, Wilke CO. 2009. Translationally optimal codons associate with structurally sensitive sites in proteins. Mol Biol Evol 26:1571-1580.

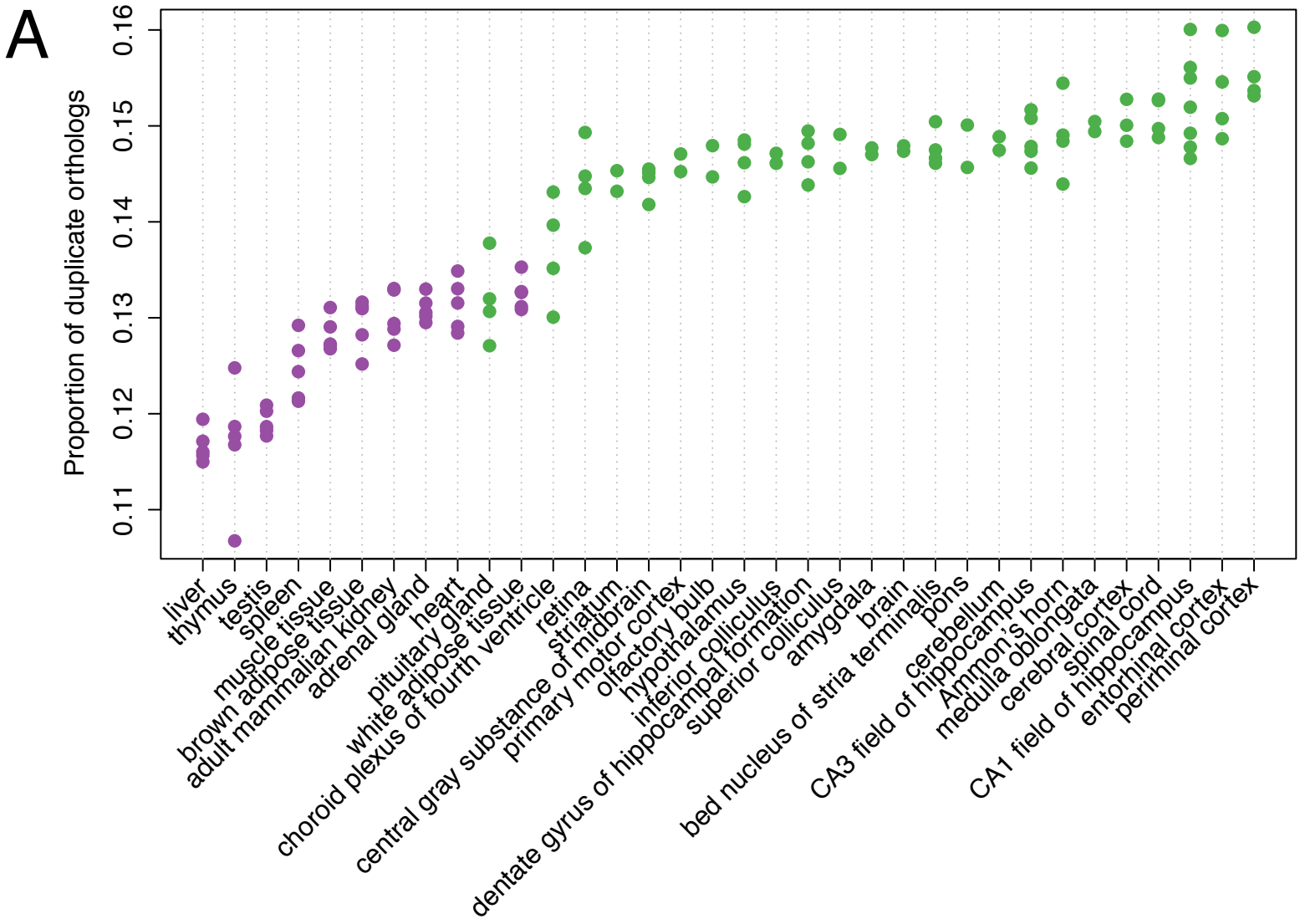
A
Proportion of duplicate orthologs
0.11
0.12
0.13
0.14
0.15
0.16
liver
thymus
testis
spleen
muscle tissue
brown adipose tissue
adult mammalian kidney
adrenal gland
heart
pituitary gland
white adipose tissue
choroid plexus of fourth ventricle
retina
striatum
central gray substance of midbrain
primary motor cortex
olfactory bulb
hypothalamus
inferior colliculus
dentate gyrus of hippocampal formation
superior colliculus
amygdala
brain
bed nucleus of stria terminalis
pons
cerebellum
CA3 field of hippocampus
Ammon's horn
medulla oblongata
cerebral cortex
spinal cord
CA1 field of hippocampus
entorhinal cortex
perirhinal cortex

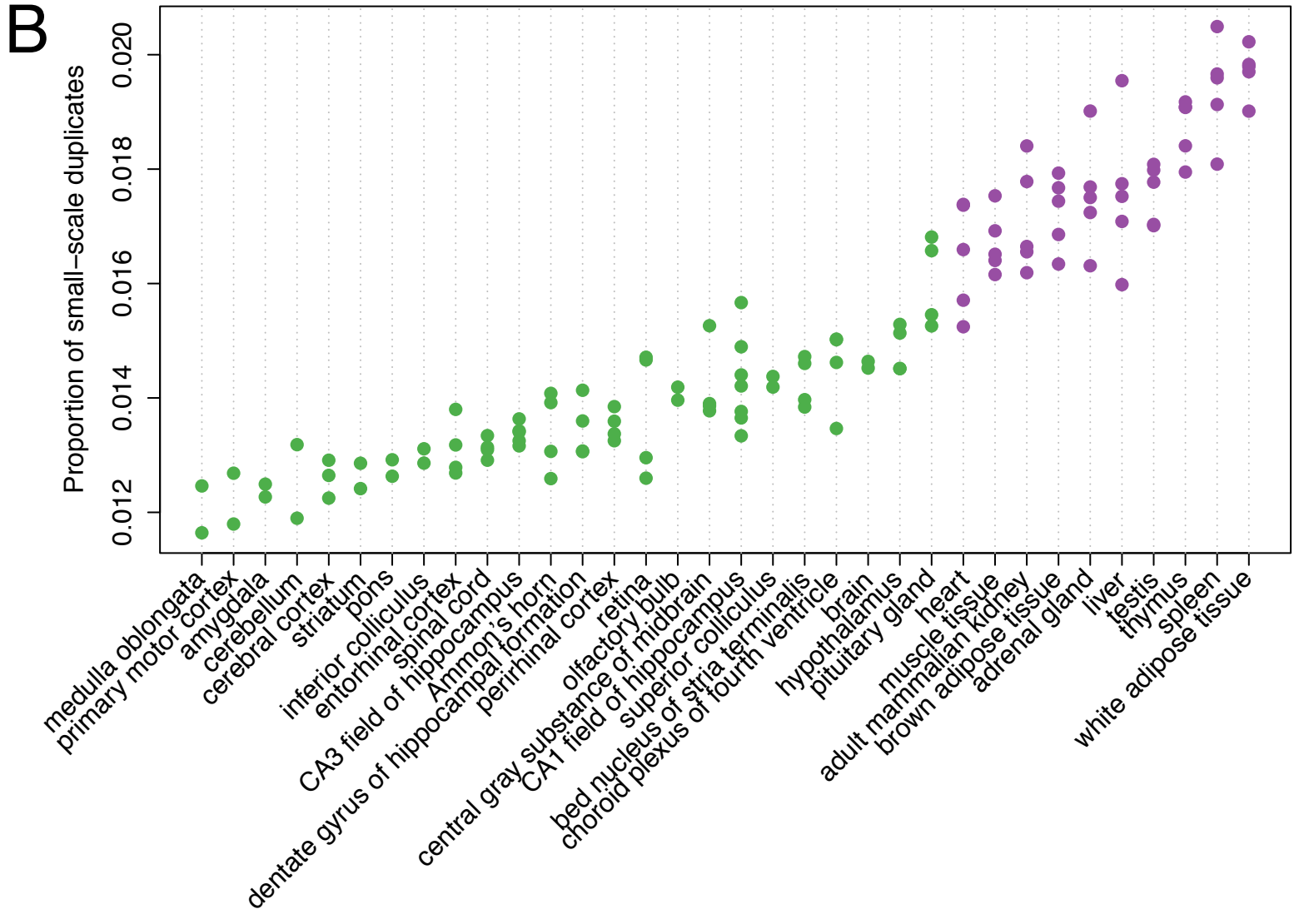
B
Proportion of small−scale duplicates
0.012
0.014
0.016
0.018
0.020
medulla oblongata
primary motor cortex
amygdala
cerebellum
cerebral cortex
striatum
pons
inferior colliculus
entorhinal cortex
spinal cord
CA3 field of hippocampus
Ammon's horn
dentate gyrus of hippocampal formation
perirhinal cortex
retina
olfactory bulb
central gray substance of midbrain
CA1 field of hippocampus
superior colliculus
bed nucleus of stria terminalis
choroid plexus of fourth ventricle
brain
hypothalamus
pituitary gland
heart
muscle tissue
adult mammalian kidney
brown adipose tissue
adrenal gland
liver
testis
thymus
spleen
white adipose tissue

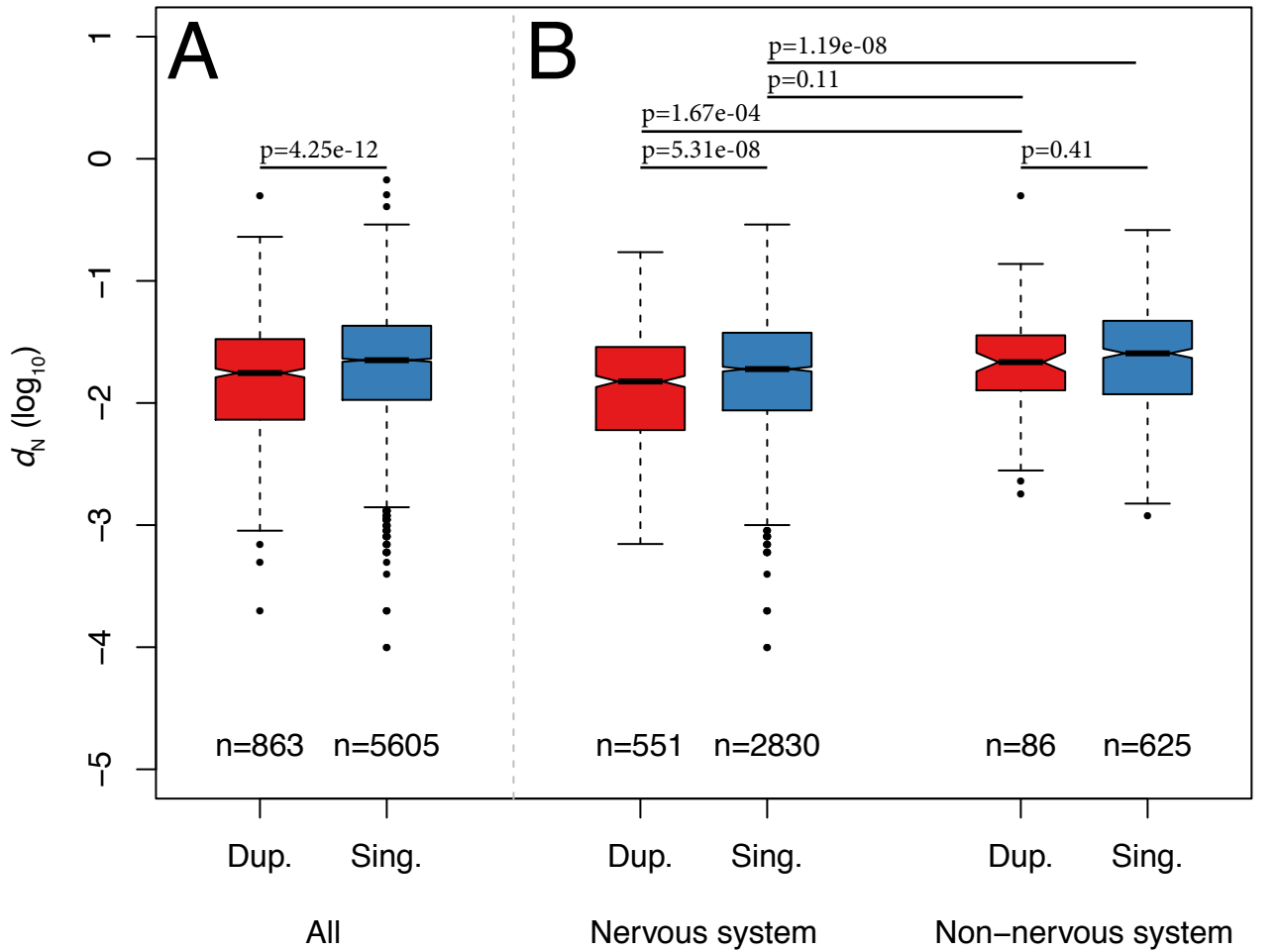
A
B
p=4.25e-12
p=1.19e-08
p=0.11
p=1.67e-04
p=5.31e-08
p=0.41
d_N ($\log_{10}$)
1
0
−1
−2
−3
−4
−5
n=863
n=5605
n=551
n=2830
n=86
n=625
Dup.
Sing.
Dup.
Sing.
Dup.
Sing.
All
Nervous system
Non−nervous system

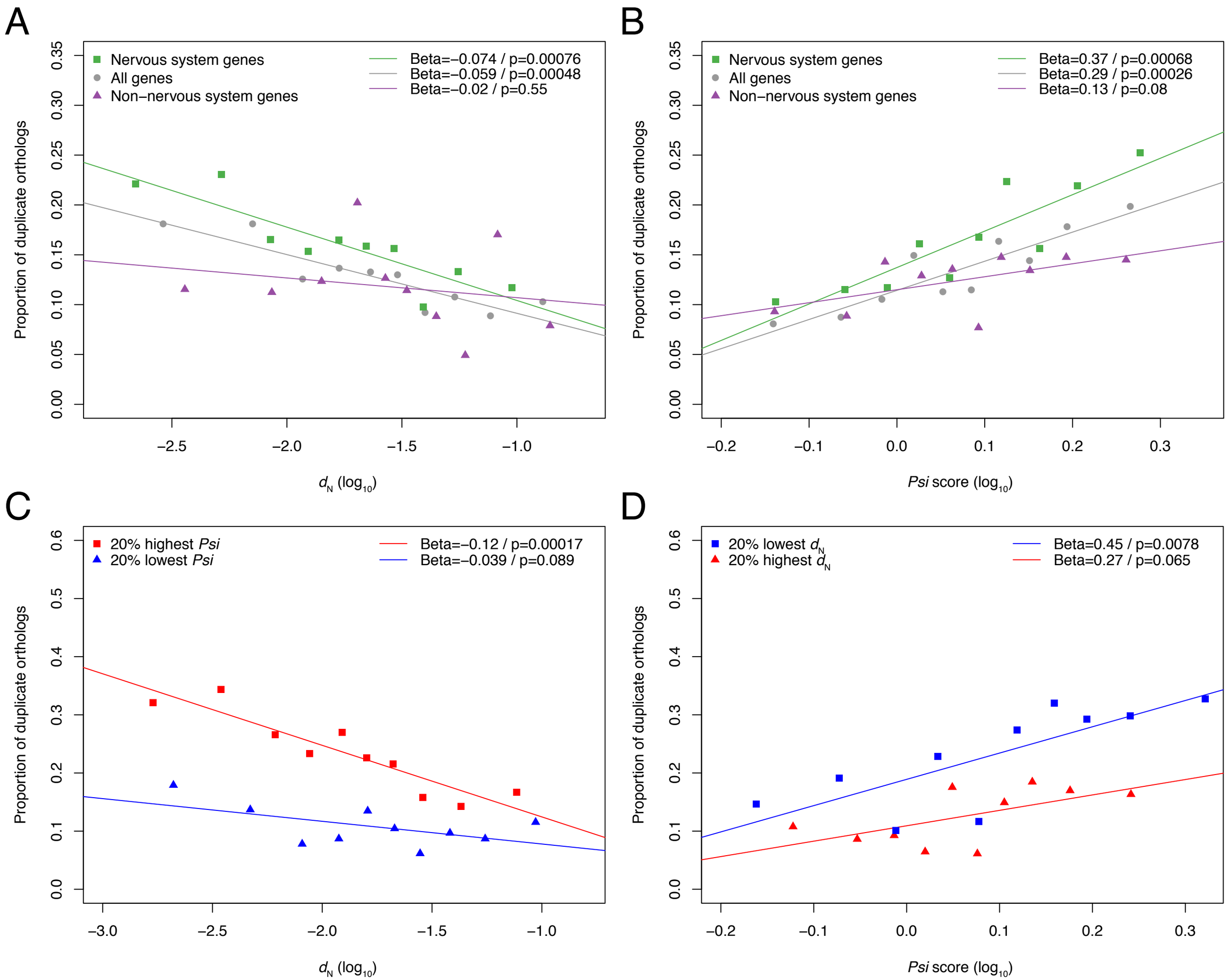
A
Nervous system genes
All genes
Non−nervous system genes
Beta=−0.074 / p=0.00076
Beta=−0.059 / p=0.00048
Beta=−0.02 / p=0.55
Proportion of duplicate orthologs
d_N (log$_{10}$)
B
Nervous system genes
All genes
Non−nervous system genes
Beta=0.37 / p=0.00068
Beta=0.29 / p=0.00026
Beta=0.13 / p=0.08
Proportion of duplicate orthologs
Psi score (log$_{10}$)
C
20% highest *Psi*
20% lowest *Psi*
Beta=−0.12 / p=0.00017
Beta=−0.039 / p=0.089
Proportion of duplicate orthologs
d_N (log$_{10}$)
D
20% lowest d_N
20% highest d_N
Beta=0.45 / p=0.0078
Beta=0.27 / p=0.065
Proportion of duplicate orthologs
Psi score (log$_{10}$)

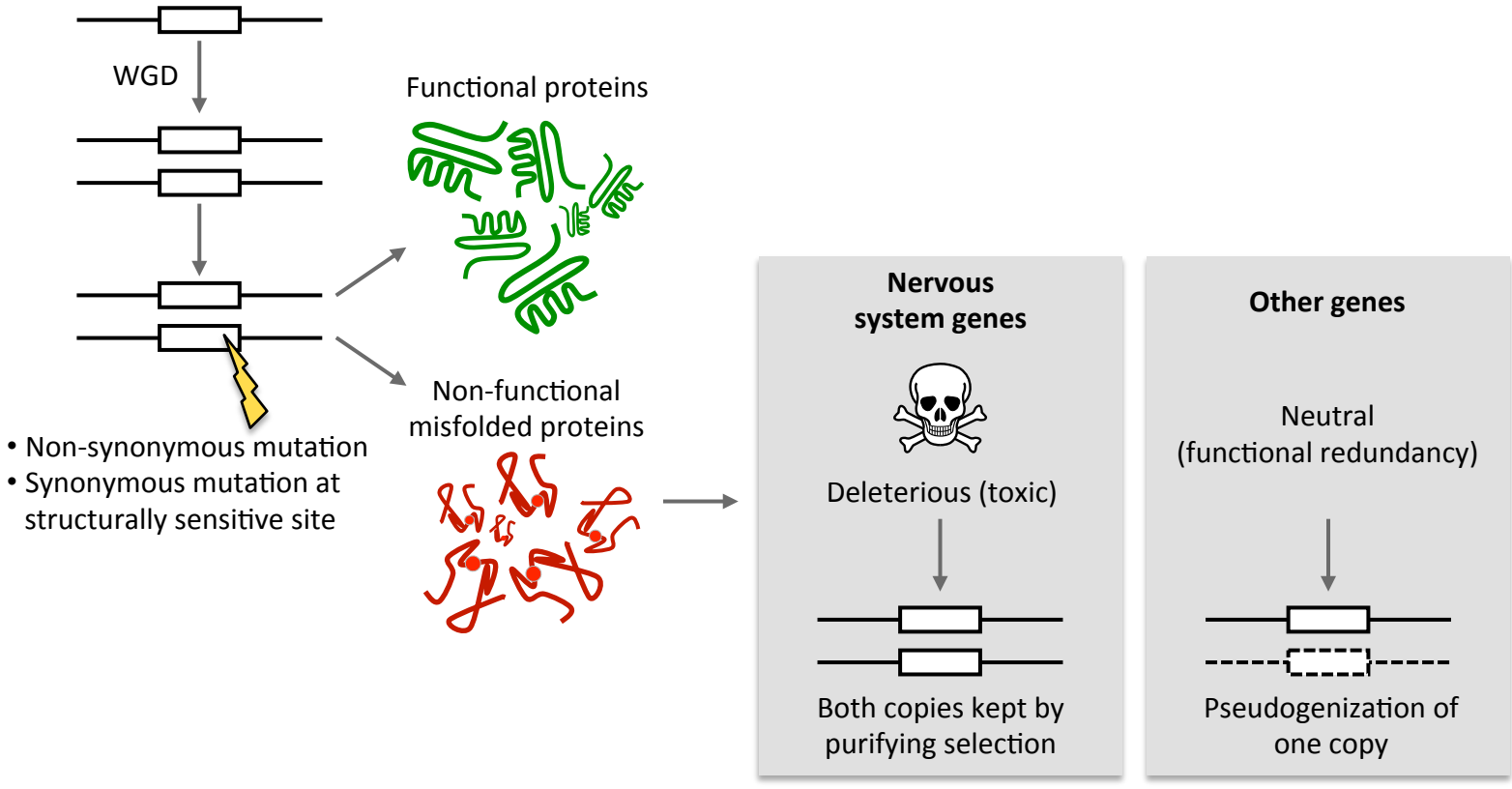
WGD
Functional proteins
Non-functional
misfolded proteins
• Non-synonymous mutation
• Synonymous mutation at
structurally sensitive site
Nervous
system genes
Deleterious (toxic)
Both copies kept by
purifying selection
Other genes
Neutral
(functional redundancy)
Pseudogenization of
one copy